Detecting anomalous crop development with multispectral and SAR time series using unsupervised outlier detection at the parcel-level: application to wheat and rapeseed crops

Florian Mouret, Mohanad Albughdadi, Sylvie Duthoit, Denis Kouamé, Guillaume Rieu, Jean-Yves Tourneret

Detecting anomalous crop development with multispectral and SAR time series using unsupervised outlier detection at the parcel-level: application to wheat and rapeseed crops⋆

Florian Mouret[a,b,*], Mohanad Albughdadi[a], Sylvie Duthoit[a], Denis Kouamé[c], Guillaume Rieu[a] and Jean-Yves Tourneret[b]

[a] *TerraNIS, 12 Avenue de l'Europe, 31520 Ramonville-Saint-Agne, France*

[b] *University of Toulouse / IRIT-INP-ENSEEIHT / TéSA, 2 Rue Charles Camichel, 31000 Toulouse, France*

[c] *University of Toulouse / IRIT-UPS, 118 Route de Narbonne, 31062 Toulouse Cedex 9, France*

ARTICLE INFO

Keywords:
Unsupervised crop monitoring
Parcel-level
Sentinel-1
Sentinel-2
Wheat crops
Rapeseed crops
Isolation Forest
Autoencoders
Outlier detection

ABSTRACT

This paper proposes a generic approach for detecting anomalous crop development at the parcel-level based on unsupervised outlier detection techniques. This approach consists of four sequential steps: preprocessing of synthetic aperture radar (SAR) and multispectral images acquired using Sentinel-1 and Sentinel-2 satellites, extraction of SAR and multispectral indicators, computation of zonal statistics at the parcel-level and outlier detection. This paper analyzes different factors that can affect the relevance of the outlier detection results for crop monitoring, such as the considered features and the outlier detection algorithm used. The proposed method is validated on rapeseed and wheat crops located in Beauce (France).

⋆This document is the results of the research project funded by TerraNIS SAS. and ANRT (convention CIFRE no. 2018/1349)

*Corresponding author
florian.mouret@terranis.fr / florian.mouret@irit.fr (F. Mouret)

1. Introduction

Remote sensing images are widely used to study the vegetation status and more specifically to monitor crop development. They have various applications in agriculture such as the extraction of agricultural information from remote sensing, phenotyping, land use monitoring and yield forecasting (Weiss et al., 2020). The link between remote sensing images, in particular multispectral and synthetic aperture radar (SAR) images, and crop vegetation has been exploited in many studies (Bannari et al., 1995; Daughtry et al., 2000; Moran et al., 2000; Wegmuller and Werner, 1997). Multispectral images have been used in various applications requiring for instance land-cover classification and biophysical parameter estimation (Gómez et al., 2016; Inglada et al., 2017; Verrelst et al., 2015a) since they are convenient to use and interpret. However, a known issue is that they are sensitive to cloud coverage and atmospheric conditions. SAR images provide more information on the vegetation structure (Abdikan et al., 2016; Betbeder et al., 2016; Khabbazan et al., 2019; Kumar et al., 2013) and are available independently from sun light conditions as well as for any cloud coverage. Note that recent reviews have mentioned the potential interest of using SAR images for vegetation monitoring (Liu et al., 2019; McNairn and Shang, 2016). Therefore, combining SAR and multispectral images is interesting because both types of images are complementary.

Challenging problems that have been addressed using multispectral and SAR images include crop classification (Inglada et al., 2016), estimation of crop water requierement (Navarro et al., 2016) and change detection (Prendes et al., 2015a,b,c). The joint use of SAR and multispectral images is also encouraged by the large amount of free data provided by Sentinel-1 (S1) and Sentinel-2 (S2) satellites operated by the European Space Agency (ESA). The fine spatial and temporal resolutions of S1 and S2 images allow working at the parcel-level with a high revisit frequency, which is well suited for precision agriculture. Crop monitoring with S1 and S2 data has already received much attention in the literature. For instance, the Sen2-Agri system uses S2 images to provide a vegetation status at the pixel level (Defourny et al., 2019). Various studies have proposed methodologies for deriving crop classification maps using S1 and S2 data (Denize et al., 2018; Kussul et al., 2018; Hedayati and Bargiel, 2018). A comprehensive analysis of the temporal behavior of S1 and S2 data has also been proposed for agricultural applications (Navarro et al., 2016; Veloso et al., 2017).

This paper addresses an interesting remaining challenge in precision agriculture, namely the automatic detection of crop parcels that have an anomalous vegetation development. This application

could for example help users such as farmers or agricultural cooperatives for optimization of agricultural practices, disease detection or fertilization management. At this point, it is worth mentioning the previous work conducted in Albughdadi et al. (2017) where agronomic indicators have been extracted from multispectral images to detect anomalies in crop parcels. However, this approach was based on the combination of missing data reconstruction and unsupervised clustering (using the mean shift algorithm), whose parameters are not easy to adjust for the detection of abnormal crop parcels. In the literature, the problem of finding objects that are unusual or different from the majority of the data is known as outlier detection (also referred to as anomaly detection). Outlier detection techniques have received a considerable attention (Aggarwal, 2017b; Chandola et al., 2009) since they are used in a large variety of application domains, *e.g.* fraud detection or medical diagnosis. In the remote sensing area, various methods have been introduced to address the problem of detecting abnormal vegetation areas at the country-level using time series constructed from the Normalized Difference Index (NDVI). These approaches aim at modeling NDVI time series using historical data and detecting potential anomalies affecting these time series by comparing new observations with their corresponding predicted values (Atzberger and Eilers, 2011; Beck et al., 2006; Klisch and Atzberger, 2016; Meroni et al., 2019; J. Verbesselt, 2012). Recent studies have investigated similar techniques with S1 and S2 data, as for instance in Kanjir et al. (2018) where Breaks for Additive Season and Trend (BFAST) is used to detect land use anomalies. However, these approaches are not particularly adapted in the case of crop monitoring. Indeed, historical modeling can be difficult because of the inconsistency of S2 time series due to the cloud coverage. There is also a lack of historical data for Sentinel satellites since the first S1 and S2 satellites were launched in 2014 and 2015, respectively. Finally, for crop monitoring it seems more important to detect the most abnormal parcels within a growing season rather than detecting inter-annual abnormalities. All these reasons motivate the need to investigate new approaches for outlier detection dedicated to crop monitoring.

Instead of using temporal models to predict potential abnormal behavior of crops (*i.e.*, techniques known as contextual outlier detection in the literature (Aggarwal, 2017b; Chandola et al., 2009)), this paper proposes to use outlier analysis methods (also referred to as point outlier detection methods in Chandola et al. (2009, Section 2.2)) that do not focus on the contextual (time) dependencies of the time series. These methods consist in comparing each instance of the dataset (here, each parcel) to the rest of the data to find the most different instances, that are isolated from the majority of the observed

data. They have been receiving an increasing interest in the literature, as outlined in the review papers Chandola et al. (2009) and Pimentel et al. (2014) and can be considered without a large amount of historical data. Moreover, multiple indicators providing information about the crop development can be used to detect outliers (not only NDVI), since no model of the normal behavior is required for the detection.

This paper studies a new outlier detection framework for crop monitoring using SAR and multispectral images acquired by S1 and S2 sensors. This detection method takes advantage of an easier access to free satellite images, especially with S1 and S2 satellites. To our knowledge, this approach is novel in the precision agriculture area as it makes use of unsupervised outlier detection algorithms within a single growing season analysis, without any prior information regarding the data behavior and using SAR and multispectral data jointly. The paper is organized as follows. Section 2 presents the study area and the data used in this work. Section 3 introduces a parcel-based outlier detection procedure for crop monitoring. Each step of this procedure is provided with practical implementation details. Section 4 validates the proposed approach on two different crop types (wheat and rapeseed crops) with a detailed analysis of the detection results. Moreover, two different parcel delineations are considered to confirm the robustness of the approach method to changes in the parcel boundaries. Finally, some conclusions and future work are reported in Section 5.

2. Study area and data

2.1. Study area

The analyzed area is located in the Beauce region in France. The area whose size is 109.8 × 109.8 km^2 is centered approximately at 48°24'N latitude and 1°00'E longitude (corresponding to the T31UCP S2 tile). Fig. 1 shows the tile location and the studied area which was chosen due to its richness of large crop fields such as wheat and rapeseed.

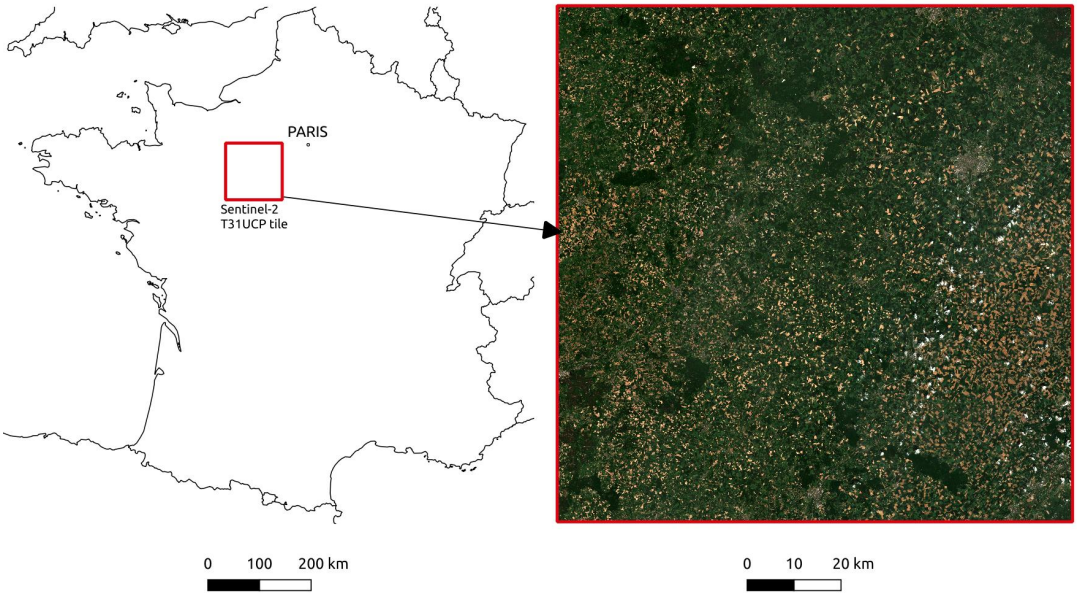

Fig. 1: The Sentinel-2 tile T31UCP considered in this work is located in the Beauce area (near Paris) and delimited by the red box. On the right, the S2 image processed in level 2A acquired the 2018-05-19.

2.2. Parcel data

The analysis presented in Sections 4.2 and 4.3 is conducted on a total of 2218 rapeseed parcels (associated with the 2017/2018 growing season) and 3361 wheat parcels (associated with the 2016/2017 growing season). The parcels discarded during the preprocessing steps detailed in what follows are not counted here. To avoid problems in parcel frontiers, a buffer of 10 m was applied allowing too small parcels (area less than 0.5 ha) to be discarded from the database. In the supplementary data attached to this paper, see Appendix A, the robustness of the proposed method to changes in the parcel boundaries is validated using 2118 rapeseed parcel delineations resulting from French Land Parcel Identification System (LPIS) which is available in open license.

2.3. Remote sensing data

The S2 and S1 images used in this study have been selected and downloaded from the PEPS platform (Plateforme d'Exploitation des Produits Sentinel) of the French National Center for Space Studies (Centre National d'Études Spatiales, CNES)[1]. Both S2-A and S2-B satellites were used, which make a theoretical revisit time of 5 days. S2 images have 13 spectral bands covering the visible, the near infra-red (NIR) and the shortwave-infrared (SWIR) spectral region (Drusch et al., 2012). Details about the spectral bands used in the analysis to extract agronomic indicators are reported in Table 1.

Table 1
Sentinel-2 multispectral bands used for the analysis.

Spectral bands	Central wavelength (μm)	Resolution (m)
Band 3: Green	0.560	10
Band 4: Red	0.665	10
Band 5: Vegetation Red Edge	0.705	20
Band 8: Near Infrared (NIR)	0.842	10
Band 11: Shortwave Infrared (SWIR)	1.610	20

Radar S1 images were acquired by a C-band synthetic aperture radar (SAR) operating at a center frequency of 5.405 GHz. Both S1-A and S1-B satellites were used in ascending orbit (6 days revisit time). Ground Range Detected (GRD) products were used in the Interferometric Wide (IW) swath mode, allowing us to work with a 10 m spatial resolution. All images were available in dual polarization (VH+VV). GRD products provide focused SAR data that have been detected, multi-looked and projected to ground range using an Earth ellipsoid model (phase information is lost but the volume of data is considerably reduced).

The acquisition dates of S1 and S2 images are depicted in Fig. 2 for the 2016/2017 and 2017/2018 growing seasons. It was decided to select S2 images with a low cloud coverage (cloud coverage lower than 20%). The strategy considered to deal with remaining clouds will be detailed in Section 3.1. For S1 images, all images covering the analyzed tile in ascending orbit were selected. For the 2016/2017 growing season, 41 S1 images and 10 S2 images were selected whereas 40 S1 images and 13 S2 images were selected in 2017/2018. Due to different cloud coverages for the two considered growing seasons, 4 images were available in June 2018 whereas only one image was available in June 2017. Also, no image was available between December 2017 and January 2018 whereas 3 S2 images were selected in 2016/2017 for the same period.

[1] `peps.cnes.fr/`, online accessed 8 July 2020

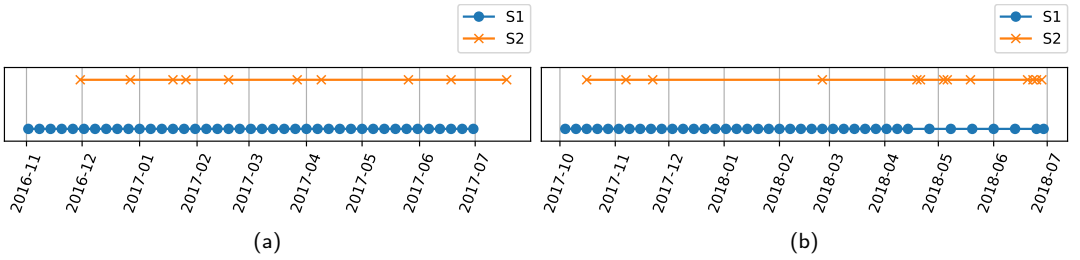

Fig. 2: Each marker correspond to the acquisition date of an used images for (a) 2016/2017 and (b) 2017/2018 growing seasons.

2.4. Generation of the reference dataset

Having access to labeled parcels is mandatory to validate the performance of the outlier detection techniques. A partial labeling of the dataset was made by analyzing the parcels detected as outliers by the different algorithms: each time a new set of features or a new algorithm tuning was tested, the parcels declared as outliers were counterchecked by experts, confirming the anomaly (true positive) or not (false positive), and determining the type of anomaly (see details later). Three main reasons motivated a partial labeling of the dataset: 1) labeling exhaustively a complete dataset would have been time consuming and not efficient because there is by definition a majority of normal parcels inside each dataset, 2) a complete labeling is not necessary to run the proposed approach since it is unsupervised 3) a relatively high amount of parcels was analyzed in each scenario in order to have a representative selection of the anomalies present in the datasets. As a consequence, the partial labeling made in this work ensures a good balance between labeling feasibility and interpretation of the results.

The labeling was conducted by photo-interpretation using all S1 and S2 images available and by using all the time series of the different indicators/statistics to compare an analyzed parcel to the rest of the data. Using time series indicators often allowed more precise interpretation of the anomalies. The different anomalies analyzed throughout the study can be decomposed into 4 main categories: heterogeneity problems, growth anomalies, database errors and others. The category "others" correspond to non-agronomic outliers that were considered as false positives and that should not be detected as they are not relevant for crop monitoring. One aim of this study is to propose the best configurations (features, algorithms) that lead to detect a minimum amount of false positive. A brief description of each category is proposed in Table 2 and more details and examples are provided below. Additional examples are also available in the supplementary data, see Appendix A.

Table 2
Description of the different categories of anomalies detected during the labeling process. Subcategories were added to have a more precise description. For each category TP means true positive, considered relevant for crop monitoring, and FP means false positive, considered irrelevant for crop monitoring.

Category (TP/FP)	Subcategory	Description
Heterogeneity (TP)	Heterogeneity	Affects the parcel most of the season
	Heterogeneity (2 different parts)	The parcel is separated into two homogeneous different parts
	Heterogeneity after senescence	Occurs during senescence
	Early heterogeneity	Occurs during early season
Growth (TP)	Late growth	A late development is observed (non-vigorous crop)
	Vigorous crop	A vigorous development is observed
	Early flowers	Early flowering phase
	Early senescence	Early senescence phase
	Late senescence	Late senescence phase
Error in database (TP)	Wrong type	A wrong crop type is reported in the database
	Wrong shape	The parcel boundaries are not accurately reported
Others **(FP)**	Normal (counterchecked)	The parcel was declared normal by the agronomic expert
	Too small	The parcel is too small, causing abnormal indicators
	SAR anomaly	Soil conditions causes abnormal SAR indicators
	Shadow perturbation (cloud or forest)	Shadows cause abnormality in the indicators.

- *Heterogeneity* corresponds to parcels presenting a clear heterogeneous development. The most common cases of heterogeneity can be observed all along the growing season and could be related for instance to soil problems, presence of weed or diseases. An example of heterogeneous parcel is shown in Fig. 3. More transient cases of heterogeneity were observed at the beginning (*early heterogeneity*) or at the end of the season (*heterogeneity after senescence*) and could be for instance related to differences in soil water content. A particular (and rare) case of heterogeneity called *Heterogeneity (2 different parts)* was observed when a parcel presents two homogeneous parts of the same crop type separated by a clear frontier, one of the two parts being affected by a delay in its development. This anomaly could be explained by different crop varieties, different seeding dates, or an error in the parcel boundaries.

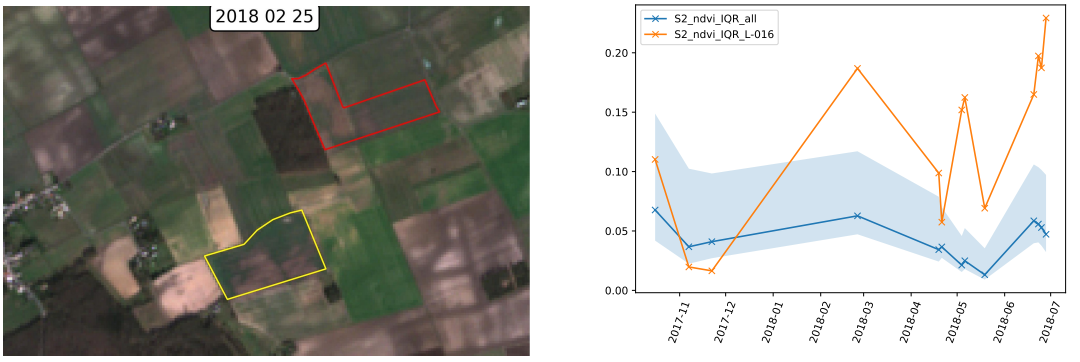

(a) (b)

Fig. 3: Example of heterogeneity affecting a parcel. (a): true color S2 image in February. (b): associated IQR NDVI time series. The blue line is the median value of the whole dataset. The blue area is filled between the 10th and 90th percentile. The orange line is the IQR NDVI for the analyzed parcel .

- *Growth anomalies* are related to an abnormal development of the parcel. It can be beneficial (*i.e.*, *vigorous crops*) or undesirable (*i.e.*, *late growth*). Fig. 4 illustrates how the different growth anomalies can affect median NDVI within a growing season and Fig. 5 provides an example of growth anomaly where S1 VH time series is affected by a late growth issue. It was observed that some highly vigorous crops are also highly homogeneous. Also, a difference between rapeseed and wheat crops was observed regarding late growth anomalies. For rapeseed crops, a late growth has generally little influence on the end of the growing season and the flowering and senescence cycle is generally normal. However, for wheat crops a late growth problem generally affects all the growing season, leading to a global low vegetation development. Finally, for wheat crops we observed few cases of vigorous crops with a majority of pixels from the red channel equal to zero for the S2 image acquired in March 27. More details regarding these observations are provided in the Supplementary Material (see Appendix A).

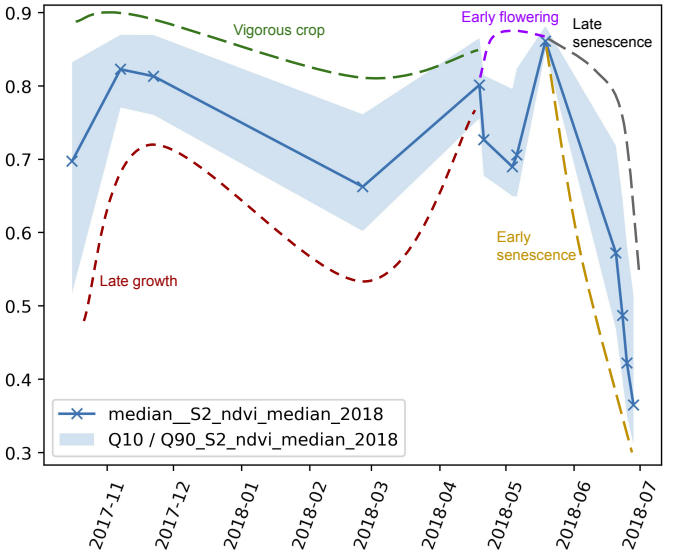

Fig. 4: Illustration of the different growth anomalies that were detected and their potential influence on the NDVI median values (rapeseed crop). The blue line is the median value of the whole dataset. The blue area is filled between the 10th and 90th percentiles. Note that in practice all the indicators were used, with median and IQR time series as well as the S1 and S2 images.

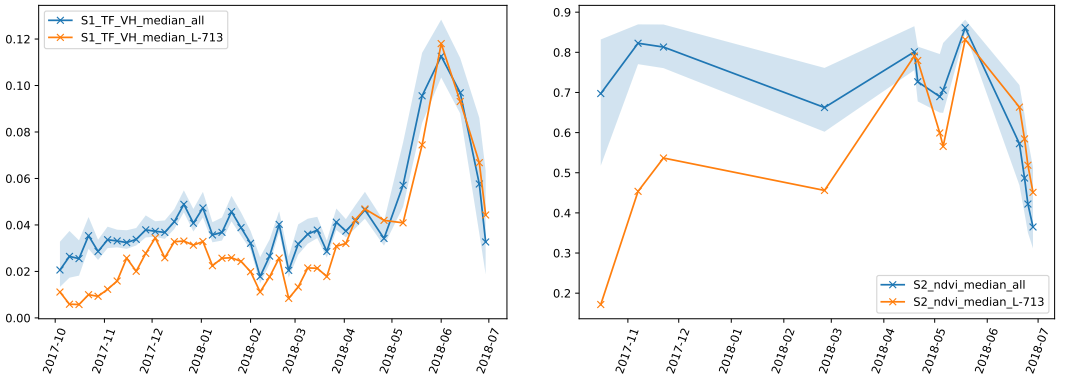

Fig. 5: Example of time series subjected to late growth for a rapeseed parcel: (a) median VH and (b) median NDVI for a rapeseed parcel. The blue line is the median value of the whole dataset. The blue area is filled between the 10th and 90th percentile. The orange line corresponds to a specific parcel subjected to late growth.

- *Database errors* are considered as relevant anomalies to be detected. This type of error is a common problem in large databases and can be challenging and time consuming to detect manually. Examples of "wrong shape" and "wrong type" reported in the database are provided in Fig. 6. This category of anomalies presents in general a strong sign of abnormality.

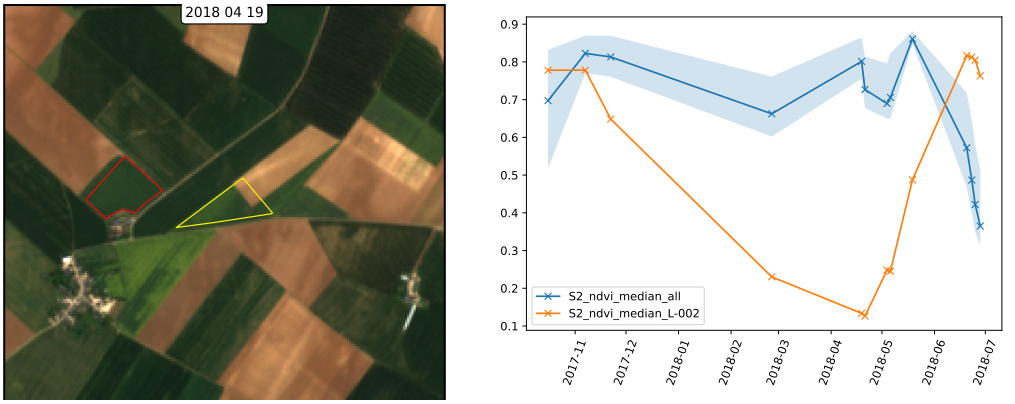

(a) (b)

Fig. 6: Two examples of error in the parcel contour database (a): an error in the parcel delineation is visible (true color S2 image). (b): median NDVI time series of a parcel with a wrong crop type reported.

- The *"Normal (counterchecked)"* label was given to parcels that were labeled as normal after inspecting the indicators and images. In some cases, some few extreme values were observed explaining why the parcel was detected as abnormal by the outlier detection algorithms. In any case, all these parcels should have an outlier score (*i.e.*, the score given by an outlier detection algorithm) lower than the parcels affected by an agronomic anomalies (*e.g.*, heterogeneity or growth anomaly).

- Other non-agronomic anomalies considered as false positive concern a few percentage of the analyzed parcels. Some very small size parcels were still present in the dataset and are labeled as *"too small"* (it is sometimes difficult to clean efficiently too small parcels that are long and narrow). Analyzing this type of parcels is not possible due to the resolution limit of Sentinel data. These parcel were kept in the database to illustrate problem that can occur in practical applications. *"Shadow"* is another kind of non-agronomic anomaly that can be caused by forests near the parcel (an example is provided in the supplementary data) or clouds (generally due to an error in the cloud mask).

- A subcategory of non-agronomic anomalies are *"SAR anomalies"*. These anomalies correspond to parcels where SAR indicators have an abnormal time evolution in early growing season (*i.e.,* the SAR indicators are abnormal compared to the rest of the data), whereas multispectral images and their indicators were counterchecked as normal. It is a known issue in crop monitoring

with SAR data that was studied in Wegmuller et al. (2006); Wegmüller et al. (2011); Marzahn et al. (2012) and reported as a "Flashing field" phenomenon. These anomalies are considered as non-agronomic since SAR data is affected by other factors than the vegetation status such as soil moisture, soil structure, row orientation or soil roughness. This kind of anomaly was observed more frequently for wheat crops and in early growing season when there is a low vegetation cover. The "flashing field" terminology can easily be understood looking at the example provided in Fig. 7.

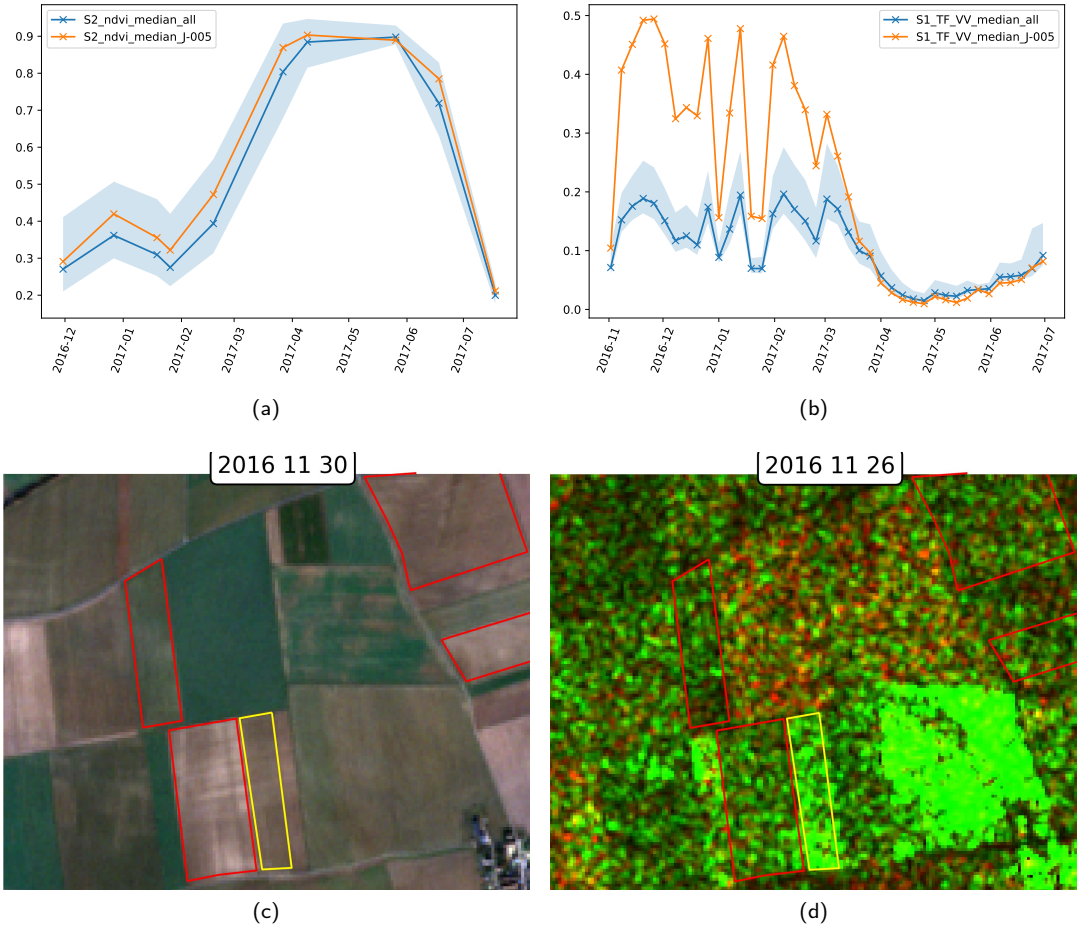

Fig. 7: Time series of (a) median NDVI and (b) median VV polarization for a wheat parcel. The blue line is the median value of the whole dataset. The blue area is filled between the 10th and 90th percentile. The orange line corresponds to a specific flashing-field parcel. Images acquired at the end of November: (c) true color S2 image and (d) S1 composite image (Green=VV, Red=VH).

Fig. 8 summarizes the distribution of the anomaly categories for both wheat and rapeseed crops, that will be used for performance evaluation. This figure shows that approximately 80% of the outliers detected during the multiple tests conducted to evaluate the proposed approach were agronomic anomalies, for both wheat and rapeseed crops. Heterogeneity and growth problems are the most detected anomalies for both types of crops, which is interesting from an agronomic point of view. Approximately 55% of the rapeseed dataset was counterchecked by the agronomic experts and at least 40% of this dataset can be considered as having relevant anomalies to be detected. The large percentage of agronomic anomalies present in this dataset can be explained by the fact that there are transient anomalies affecting a limited time interval of the growing season. These anomalies are for instance delays during the senescence phase. Fewer tests were made with the wheat dataset but almost 25% of the parcels was counterchecked.

3. Proposed method

The outlier detection method proposed in this paper consists of four sequential steps depicted in Fig. 9 and discussed in detail in what follows.

3.1. Image preprocessing

S2 images were preprocessed using the online MAJA processing chain (Hagolle et al., 2015) available on the PEPS platform of CNES. This preprocessing step provides bottom-of-the atmosphere level-2A ortho-rectified products expressed in surface reflectance. In addition to atmospheric correction, Level-2A images are available with a cloud mask discarding cloud pixels in the images. A resampling strategy was adopted to obtain a spatial resolution of 10 m for the channels with a lower spatial resolution. Parcels fully covered by clouds during at least one time instant were discarded from the database and parcels partially covered by cloud were analyzed using pixels not covered by the cloud mask.

To build the database of S1 images, an offline processing illustrated in Fig. 10 was conducted with the Sentinel Application Platform (SNAP, version 7.0)[2]. This processing is inspired by the workflow proposed in Filipponi (2019). However, a Terrain-Flattening operation was added to take into account the local incidence angles as the analyzed area is wide and parcels indicators are compared to each others. This operation uses the Shuttle Radar Topography Mission (SRTM) Digital Elevation Model (DEM). The Range Doppler terrain correction provides orthorectified images. Note that a

[2] `http://step.esa.int/main/toolboxes/snap/`, online accessed 8 July 2020

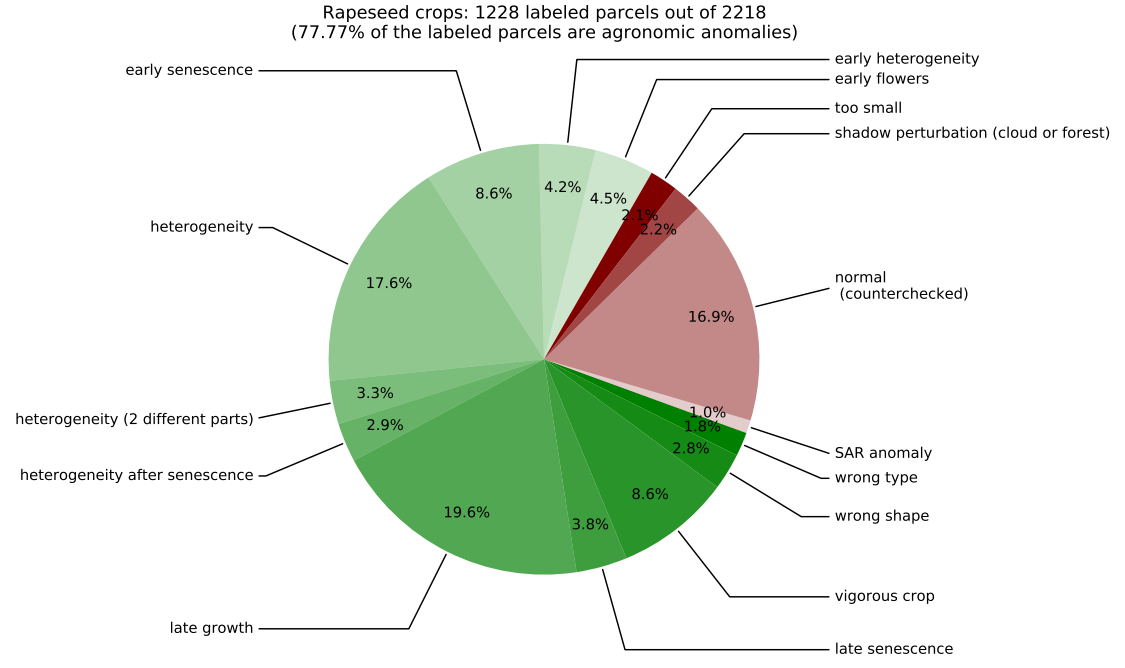

(a)

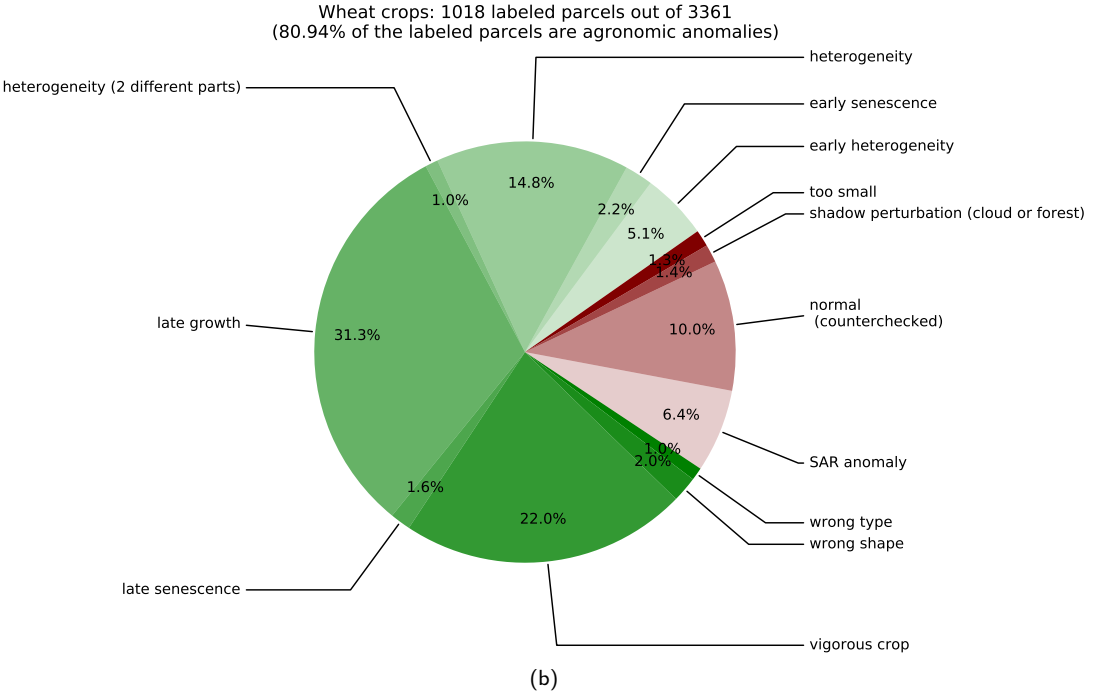

(b)

Fig. 8: Pie charts representing the distribution of the labeled parcels for (a) wheat crops and (b) rapeseed crops. Green categories correspond to relevant anomalies considered as true positive. Red categories correspond to non-agronomic anomalies considered as not relevant.

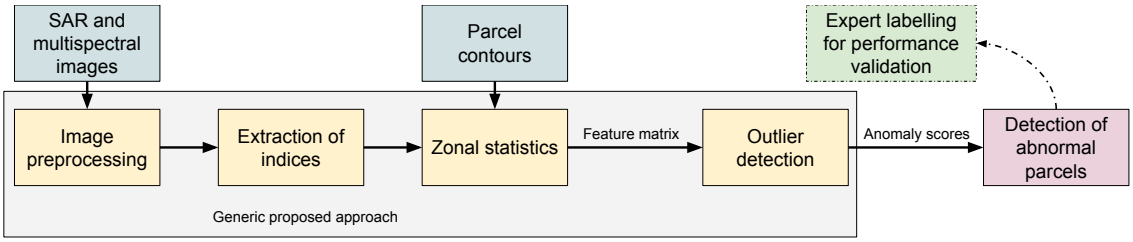

Fig. 9: Diagram summarizing the main steps of the proposed approach.

multi-temporal speckle filtering step was also tested without significant differences on the results (we implemented our own Python version of the filter proposed in formula (14) in Quegan and Jiong Jiong Yu (2001)). The best results were obtained with the presented workflow.

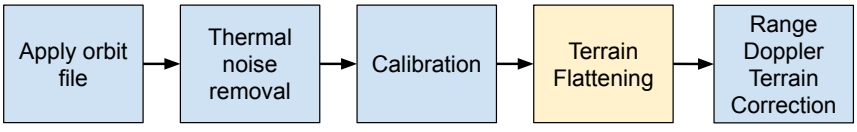

Fig. 10: Sentinel-1 processing graph used in Sentinel Application Platform (SNAP). The yellow box, terrain flattening, was added to the workflow proposed in Filipponi (2019) to take into account the local incidence angle.

3.2. Extraction of SAR and multispectral indicators

The following section describes the indicators derived from multispectral and SAR images considered in this work (reported in Table 3) and their importance for monitoring crop growth. In practice, an unsupervised algorithm is likely to use all the features available for the analysis and we have observed that choosing irrelevant features can lead to bad detection results. Consequently, the indicators used in the study were selected because they are related to the vegetation status. Note that raw S2 bands were also tested without improvement of the detection precision and a harder interpretation of the results when compared to vegetation indices.

3.2.1. Multispectral vegetation indices

Many multispectral Vegetation Indices (VIs) have been proposed in the literature *e.g.*, (Bannari et al., 1995; Wu et al., 2008). A VI relates the acquired spectral information to the observed vegetation, and thus allows better quantitative and qualitative evaluations of the vegetation covers. It is also important to choose indicators whose interpretation is easy, in order to understand why an anomaly has been detected. Our objective is not to analyze the various VIs available in the literature for crop

monitoring but rather to propose a generic approach for detecting anomalies in different crops. This paper considers five multispectral VIs reported in Table 3 and described below.

The Normalized Difference Vegetation Index (NDVI) is a benchmark indicator for agronomic analysis that is mainly related to the plant vigor (Rouse et al., 1974; Bannari et al., 1995). The Normal Difference Water Index (NDWI) actually refers to two different widely used indicators. The first version uses Near infrared (NIR) and Short Wave infrared (SWIR) to monitor changes in the water content of leaves (Gao, 1996). The second version uses the green band and NIR to monitor changes related to content in water bodies (McFeeters, 1996). Both formulas are similar to NDVI with different bands involved. The SWIR version of NDWI seems to be more appropriate for crop analysis but the GREEN version of NDWI can also provide relevant information, *e.g.*, for flooded parcels. The Modified Chlorophyll Absorption Ratio Index (MCARI) was designed to extract information from the chlorophyll content in plants with a resistance to the variation of the Leaf Area Index (LAI). A variant called MCARI/OSAVI is using the Optimized Soil Adjusted Vegetation Index (OSAVI) to minimize the contribution of background reflectance (Wu et al., 2008; Daughtry et al., 2000). The Green Red Vegetation Index (GRVI) is similar to NDVI but uses the red and green bands. According to Motohka et al. (2010), GRVI "*can be a site-independent single threshold for detection of the early phase of leaf green-up and the middle phase of autumn coloring*" (referred to as senescence for crops).

3.2.2. SAR indicators

Many works have been performed to establish a relationship between SAR images and vegetation. One can mention for instance two recent reviews reporting the advances in this area of investigation (McNairn and Shang, 2016; Liu et al., 2019). The relationship between SAR and vegetation is not straightforward as other factors such as soil moisture or soil structure also impact SAR signals. A Radar Vegetation Index (RVI) was developed in Kumar et al. (2013) but it requires quad-polarizations that are not available with S1 images. The backscattering coefficients (denoted as γ^0_{VH} and γ^0_{VV}) have been used intensively in the literature as for example in Whelen and Siqueira (2018); Khabbazan et al. (2019). Their ratio $\gamma^0_{\mathrm{VH}}/\gamma^0_{\mathrm{VV}}$ has also been used for vegetation analysis (Denize et al., 2018; Abdikan et al., 2016) as it has the advantage of counterbalancing the effect of soil moisture (Veloso et al., 2017; Vreugdenhil et al., 2018). However, we did not observe any improvement when adding this indicator in the outlier analysis and using it alone lead to poor detection results. To that extent, results using this ratio will not be presented here.

Table 3
Vegetation indices computed from S2 images and SAR indicators computed from S1 images used in this paper. For S2, The near infrared (band 8), red edge (band 5), short wave infrared (band 11), green (band 3) and red (band 4) channels are denoted as NIR, RE, SWIR, GREEN and RED, respectively.

Sensor type	Indicator	Formula
Multispectral	NDVI	$\frac{\text{NIR}-\text{RED}}{\text{NIR}+\text{RED}}$
	$\text{NDWI}_{\text{SWIR}}$	$\frac{\text{NIR}-\text{SWIR}}{\text{NIR}+\text{SWIR}}$
	$\text{NDWI}_{\text{GREEN}}$	$\frac{\text{GREEN}-\text{NIR}}{\text{GREEN}+\text{NIR}}$
	$\frac{\text{MCARI}}{\text{OSAVI}}$	$\frac{(\text{RE}-\text{IR})-0.2(\text{RE}-\text{RED})}{(1+0.16)\frac{\text{NIR}-\text{RED}}{\text{NIR}+\text{RED}+0.16}}$
	GRVI	$\frac{\text{GREEN}-\text{RED}}{\text{GREEN}+\text{RED}}$
SAR	Cross-polarized backscattering coefficient VH	γ^0_{VH}
	Co-polarized backscattering coefficient VV	γ^0_{VV}

3.3. Input data for the outlier detection algorithms

3.3.1. Zonal statistics

The proposed approach detects crop anomalies at the parcel-level, through appropriate statistics referred to as "zonal statistics" (*i.e.*, spatial statistics) that are computed from S1 and S2 indicators. Zonal statistics summarize the information contained in each parcel whose delineation is reported in the database. Multiple statistics were considered such as the median, interquartile range (IQR), skewness and kurtosis. The median allows the mean behavior of a parcel to be captured with more robustness than the classical mean as it is not affected by extreme values (Huber, 2011) and can thus detect global anomalies such as anomalies in crop vigor. On the other hand, IQR contains important information related to heterogeneity. IQR is defined as the difference between the 75th and 25th percentiles, which helps to detect large heterogeneous growth conditions within a parcel when computed using S2 images[3] while being robust to the presence of extreme values. The skewness aims at measuring the asymmetry of a distribution whereas the kurtosis can be used to characterize the tail of a

[3]Note that the IQR of S1 data is directly proportional to the median, and thus does not bring any additional information compared to the median.

distribution. Both measures are complementary to median and IQR to analyze the distribution of the pixels within a crop parcel. These statistics were extracted for each indicator at each date for each parcel using the python libraries SciPy version 1.4.1 (Virtanen et al., 2020) and rasterstats version 0.13.0[4]. As mentioned in Section 3.1, cloud pixels were discarded meaning that these statistics were computed from pixels not filtered by the cloud mask.

3.3.2. Feature matrix

From the zonal statistics of the different indicators computed at different dates, a feature matrix is constructed and used as the input of outlier detection algorithms. Each parcel is represented by a vector concatenating all the statistics computed for the different indicators at different dates. The number of features for a given parcel is $N_f = N_{1,im} \times N_{1,ind} \times N_{1,s} + N_{2,im} \times N_{2,ind} \times N_{2,s}$, where $N_{1,im}$ is the number of S1 images, $N_{1,ind}$ is the number of indicator extracted for each S1 image, $N_{1,s}$ is the number of statistics computed for each S1 indicator and similar definitions apply to $N_{2,im}$, $N_{2,ind}$ and $N_{2,s}$ for S2 images. For instance, in 2017/2018, if all S1 and S2 images are used and two statistics (median/IQR) are computed for all the indicators (5 multispectral indicators and 2 SAR indicators), the number of features is equal to $N_f = 290$. Various sets of features were tested and analyzed as presented in the next section. The construction of the feature matrix is illustrated in Table 4 when using a unique indicator NDVI with 2 statistics. As each column corresponds to a unique combination statistics/indicator/time, it is possible to compare each parcel columnwise. Note that classical preprocessing such as Principal Component Analysis (PCA) (Jolliffe, 1986) or Multidimensional Scaling (MDS) (Borg and Groenen, 1997) were applied to this feature matrix without significant improvement regarding the outlier detection results. Thus, these preprocessing were ignored from our analysis.

Table 4
Simplified version of the feature matrix using NDVI only and two statistics (median/IQR) for n dates and M parcels. NDVI_{t_n} means NDVI computed for image #n and median_{P_M} means spatial median of the indicator computed inside the parcel #M

Parcel #	Feature 1	Feature 2	.	Feature L-1	Feature L
P_1	$\text{median}_{P_1}(\text{NDVI}_{t_0})$	$\text{IQR}_{P_1}(\text{NDVI}_{t_0})$	.	$\text{median}_{P_1}(\text{NDVI}_{t_n})$	$\text{IQR}_{P_1}(\text{NDVI}_{t_n})$
P_2	$\text{median}_{P_2}(\text{NDVI}_{t_0})$	$\text{IQR}_{P_2}(\text{NDVI}_{t_0})$	.	$\text{median}_{P_2}(\text{NDVI}_{t_n})$	$\text{IQR}_{P_2}(\text{NDVI}_{t_n})$
...	...	...	.	...	...
P_M	$\text{median}_{P_M}(\text{NDVI}_{t_0})$	$\text{IQR}_{P_M}(\text{NDVI}_{t_0})$	.	$\text{median}_{P_M}(\text{NDVI}_{t_n})$	$\text{IQR}_{P_M}(\text{NDVI}_{t_n})$

[4] https://pythonhosted.org/rasterstats/, online accessed 8 July 2020

3.4. Outlier detection algorithms

Four benchmark outlier detection algorithms are tested in this paper: One-Class Support Vector Machine (OC-SVM) (Schölkopf et al., 1999), Local Outlier Probabilities (LoOP) (Kriegel et al., 2009), Isolation Forest (IF) (Liu et al., 2012), and AutoEncoder (AE) (Aggarwal, 2017b, Section 3.6). These algorithms are based on different ideas, making them interesting for comparison purposes. To run the experiments conducted in this study, the Python Scikit-learn (version 0.23.0) implementations of OC-SVM and IF were used (Pedregosa et al., 2011). The Python library PyNomaly (version 0.3.3) was used for the implementation of the LoOP algorithm (Constantinou, 2018). Finally, we implemented our own autoencoder with the Python library Keras[5] (version 2.3.0).

The LoOP algorithm (Kriegel et al., 2009) is an unsupervised outlier detection method based on the nearest neighbors of the observed samples. It is an extension of the Local Outlier Factor (LOF) algorithm (Breunig et al., 2000). The main idea behind LoOP is that normal data instances occur in dense neighborhoods and anomalies occur far from their closest neighbors (Chandola et al., 2009). This algorithm compares the local density of each instance with that of its k-nearest neighbors (knn). For LoOP, two hyperparameters have to be fixed: k, the number of nearest neighbors and the "extent" parameter denoted as λ. This parameter defines the statistical notion of an outlier as an object deviating more than a given λ times the standard deviation from the mean (Constantinou, 2018).

OC-SVM (Schölkopf et al., 1999; Tax and Duin, 2004) is a model-based technique, which assumes that all training instances are part of the same class delimited by a separating boundary and that the instances that are not inside the learned boundary are anomalies (Chandola et al., 2009). A kernel can be used to transform the OC-SVM linear model into a non-linear model as for the classical SVM method. A Radial Basis Function (RBF) kernel was investigated in this paper, the choice of this kernel was mainly motivated by its effectiveness that has been observed in many different practical applications (Schölkopf et al., 2004; Kuo et al., 2014). The RBF kernel has a single hyperparameter referred to as kernel bandwidth and denoted as σ which has to be adjusted for each dataset. In the OC-SVM algorithm, an upper bound for the fraction of training samples located outside the frontier denoted ν has to be fixed by the user. The choice of this bound can largely influence the behavior of the classifier (Schölkopf et al., 1999; Pimentel et al., 2014). Moreover it implies that outlier scores can change according to the amount of anomalies to be detected (called the outlier ratio) which is fixed by

[5] `https://keras.io/`, online accessed 8 July 2020

the parameter ν. This can be a disadvantage for practical applications compared to the other algorithms of the study which compute a unique outlier score for each instance independently from the amount of abnormal parcels to be detected. Thus it is possible to select the percentage of anomaly to be detected by sorting the instances using their outlier scores whereas for OC-SVM a new outlier detection has to be run when changing the amount of parcel to be detected.

The IF algorithm (Liu et al., 2008) uses a new concept called isolation that aims at detecting anomalies without using any distance or density measure, assuming that outliers can be isolated more easily than other instances. Using binary isolation trees to separate instances, outliers are more likely to be isolated at the root of the trees whereas inliers tend to be isolated at deeper parts of the trees. The IF algorithm constructs multiple random isolation trees defining a so-called forest of iTrees. At each node, a random feature is chosen with a random split value. When using random splits with random features, outliers are more likely to be isolated first. The IF algorithm is known to be very fast compared to other algorithms (especially for large datasets) since it does not compute a pairwise distance matrix.

AEs have been considered intensively for feature learning and dimensionality reduction (Kramer, 1991) and have been popularized thanks to the advent of deep learning (LeCun et al., 2015). Similar to other dimensionality reduction techniques such as PCA (Jolliffe, 1986), AEs can be used for outlier detection: the idea is that outliers tend to have a greater reconstruction error compared to nominal vectors (Aggarwal, 2017b). AEs are able to learn a non-linear representation of the data for classification or outlier detection. However, they tend to be subject to overfitting issues and sometimes need a large amount of parameter tunings to work efficiently (*e.g.*, number of hidden layers, choice of activation functions, selection of regularization parameters, loss definition, number of epochs for training, batch size). Note that other deep outlier detection methods, such as Variational Autoencoders (VAE) (An and Cho, 2015) were also tested but without providing significant improvement compared to standards AEs.

3.5. Performance evaluation

The labeled dataset introduced in Section 2.4 allows the performance of the different outlier detection algorithms for various sets of features to be compared. This section provides some quantitative measures that have been used for this comparison. The precision can be used to evaluate the quality

of the results and is defined as

$$\text{precision} = \frac{\text{TP}}{\text{TP} + \text{FP}} \tag{1}$$

where TP and FP are the numbers of true positives and false positives, respectively. The precision expresses the percentage of detected parcels that are true positives (here, agronomic anomalies). Ideally, the precision should be as high as possible. A major limitation of using precision alone is that it does not provide information regarding the non-detected parcels. Indeed, it is possible to have a good precision even if a lot of actual anomalies are not detected.

Another efficient way to compare various sets of features and different outlier detection algorithms is to plot the precision against the outlier ratio. The outlier ratio is defined as the percentage of anomalies to be detected by the algorithm. For a given outlier ratio, a good algorithm or feature choice will globally have detection results with a higher precision. In our case, because we do not know the percentage of anomalies to be detected as it depends on the user's needs, these curves are interesting for comparison purposes. These curves are similar to the Receiver Operating Characteristics (ROC) but have the advantage to be more adapted to outlier detection (*i.e.*, a maximum outlier ratio can be fixed in order to keep realistic conditions). We observed that both types of curves lead to the same conclusions, with an easier interpretation for the precision vs. outlier ratio curves. The area under the precision vs. outlier ratio curve (AUC) can be used to easily compare different anomaly detection results. In the analysis, we computed the AUC for outlier ratios in the range [0, 0.5] in order to focus on realistic values of the number of outliers. The AUC was then divided by 0.5 to normalize the obtained value: the score provided can be seen as the average precision for outliers ratios in the range [0, 0.5]. One limitation is that this representation does not give information regarding the distribution of the different detected categories. Two algorithms can have the same precision without detecting the same parcels (*e.g*, one algorithm can detect more heterogeneous parcels whereas another one detects more late growth anomalies). Using the distribution of the different types of anomalies detected for a given outlier ratio is a complementary way to address this limitation.

3.6. Conducted experiments

In this study, various experiments are conducted to 1) evaluate the proposed procedure and its relevance for crop monitoring and 2) understand which factors have an influence on the detected anomalies.

To that extent, different sets of features and algorithms are compared with different initial configurations, which are reported in Table 5. Moreover, various tests are made for analyzing a complete growing season (*i.e.*, using all the images available for a season) to detect anomalies in the rapeseed and wheat parcels. Analyzing the data from a complete season is interesting to evaluate the capacity of the proposed approach to detect anomalies occurring at different periods of the crop growth, and to determine whether differences between the detected parcels are observable or not. Some other tests are also made with a lower amount of data (and in particular for a mid season analysis between October and February). Early detection can be of interest for warning purposes at the beginning of the growth cycle and gives more details on the effect of having only few data available for the analysis. The influence of the amount of parcels to be detected (called outlier ratio) is also tested to analyze the relevance of the outlier score given to each parcel. A total number of 250 different experiments were made for rapeseed crops to evaluate the different factors reported in Table 5. Fewer experiments were made with the wheat dataset because the main idea was to determine whether the proposed algorithm can be applied with minor modifications to other kinds of crops or not.

Table 5
Summary of the different experiments conducted in the study to evaluate the proposed approach. Evaluated factors in italics are not shown in this documents but were considered during our analysis.

Evaluated crop type	Time interval	Section	Evaluated factors
Rapeseed	Complete season	4.2.1	Outlier detection algorithms
		4.2.2	Feature sets
		4.2.3	Outlier ratio
		4.2.4	Zonal statistics
		4.2.5	S1 features alone
		4.2.6	Missing S2 images
		Supl.	*(changes in parcel boundaries)*
	Mid season	4.2.7	Feature sets *(algorithms, S1 alone, outlier ratio)*
Wheat	Complete season	4.3	Feature sets, S1 alone *(algorithm, outlier ratio)*
	Mid season	-	*(algorithm, feature sets, S1 alone, outlier ration)*

The different feature combinations tested in this study are identified using abbreviations that are defined in Table 6 with representative examples. Each set of features is labeled using the indicators and statistics used for both S1 and S2 sensors.

Table 6
Examples of abbreviations with their corresponding sets of features used for outlier detection.

Abbreviated name	Features used
S2: all (median / IQR)	Median and IQR of the 5 S2 indicators listed in Section 3.2
S2: NDVI (median / IQR)	Median and IQR of NDVI
S2: all (median / IQR), S1: VV, VH (median)	Median and IQR of the 5 S2 indicators and median of the 2 S1 indicators VV and VH.

4. Results and discussion

This section presents detailed results about anomaly detection for rapeseed and wheat parcels. Note that two different sets of features or algorithms sometimes provide similar results which means that the global process is robust to changes and that different initial configuration can lead to the same conclusions.

4.1. Hyperparameter tuning

This section summarizes the different hyperparameter tunings that have been considered for each algorithm leading to the values reported in Table 7.

For LoOP algorithm, the number of *knn* was fixed by grid search to $k = 701$. This value provided detection results of higher precision compared to the other tested values (note that small changes in the value of k do not significantly affect the result). It was found that choosing a too small number of neighbors (*e.g.*, choosing an odd-valued integer close to the square root of the number of observations as proposed in Constantinou (2018)) leads to detect too subtle anomalies that are not related to agronomic issues. The extent parameter of LoOP was fixed to $\lambda = 2$ as recommended in Constantinou (2018) since it did not have a significant influence on the detection results.

For the OC-SVM algorithm, an efficient heuristic (Jaakkola et al., 1999; Aggarwal, 2017a) consists of estimating the parameter σ as the median of the pairwise Euclidean distances between vectors from the learning set $\mathcal{X}$, denoted as median(dist($\mathcal{X}$)). This estimator of σ presented provided good results without a need to a manual tuning for each new dataset.

The IF algorithm was used with a number of iTrees equal to $n_{trees} = 1000$ and a subsampling fixed to $n_{samples} = 256$ as in the original paper (Liu et al., 2008). Changing these two parameters did not have a significant effect on the results, which is a crucial advantage compared to the other algorithms.

Indeed, it seems that the IF algorithm does not require a fine hyperparameter tuning. It is important because in real conditions, a bad tuning of the hyperparameters generally leads to poor results for an unsupervised detection method, which is not the case for the IF method.

The parameters of the AE were tuned by grid search. We considered a classical structure similar to the one proposed in the Python library for outlier detection PyOD (Zhao et al., 2019): 4 hidden layers with respectively 64, 32, 32 and 64 neurons. A Relu activation function was used for all layers except for the output using a sigmoidal function. The layer's output regularization parameter of the algorithm (referred to as "activity regularizer" in Keras) was set to 10^{-5}. Note that this specific regularization significantly improved the detection results, contrary to changes in the network structure (e.g., number of neurons).

Because they are using distances, the OC-SVM, LoOP and AE algorithms also require a normalization in order to have input features in the interval [0, 1], while this step is not mandatory when using the IF algorithm.

Table 7
Hyperparameters used in the different algorithms

Algorithm	Hyperparameter	Value
IF	n_{trees}	1000
	$n_{samples}$	256
LoOP	k	701
	λ	2
AE	hidden neurons	64, 32, 32, 64
	output regularization	10^{-5}
OC-SVM	σ	median(dist($\mathcal{X}$))

4.2. Anomaly detection results for rapeseed crops (2017/2018)

In what follows, unlabeled parcel are considered as false positives when displaying the precision vs. outlier ratio curves. It has for effect to potentially underestimate the precision values, but it seems reasonable to consider as false positives parcels that were never detected after more than 250 experiments. For outlier ratios lower than 20%, all the parcels are labeled (if not mentioned). For higher outlier ratios values, a majority of labeled parcels are generally still detected with high precision values.

4.2.1. Effect of the algorithm used for crop anomaly detection

The performance of the different outlier detection algorithms (AE, LoOP, OC-SVM and IF) was first tested for a complete season analysis. A first experiment was made by computing precision vs.

outlier ratio curves for the different algorithms. As explained in Section 3.4, the OC-SVM algorithm does not provide a unique outlier score associated with each parcel as it depends on the maximum amount of outliers defined by the parameter ν. For the other algorithms, an anomaly score is attributed to each parcel and it is then possible to choose the outlier ratio by sorting the parcels according to their anomaly score (in order to select an appropriate percentage of parcels to be detected). Fig. 11 shows that all the outlier detection algorithms provide similar precision for outlier ratios lower than 30% with a majority of relevant anomalies detected (more than 90%), confirming that multiple methods can lead to similar accuracy. The outlier ratio is plotted up to 0.5 to highlight the differences when detecting a large amount of outliers, which is possible for a complete growing season as various transient anomalies can occur. IF and AE perform slightly better overall with a higher AUC and the IF outlier score is more relevant for outlier ratio greater than 30%.

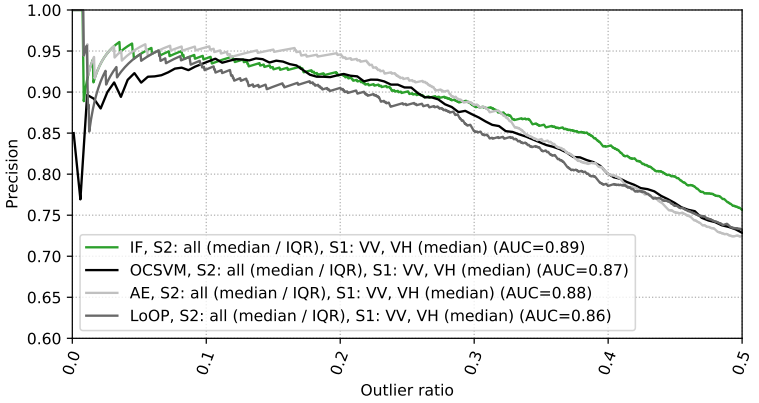

Fig. 11: Precision vs. outlier ratio for a complete growing season analysis of the rapeseed parcels. Various algorithms are compared using the same set of features. The abbreviations used in the legend are defined in Table 6.

To analyze potential differences within the anomaly categories detected, the 4 algorithms were run with an outlier ratio fixed to 20%. The percentages of the detected parcels within each category for LoOP, OC-SVM, AE and IF are displayed in Fig. 12. Overall, all the algorithms detect a majority of heterogeneity (34% for IF) and late growth (25% for IF) anomalies, which can be understood as these anomalies generally affect the complete growing season. It also appears that almost all the "wrong type" and "wrong shape" of the dataset are detected, which seems also logical as these anomalies strongly affect the parcel's time series. The histograms obtained with LoOP and IF are very similar, whereas OC-SVM and AE seems to detect less heterogeneity anomalies (44 heterogeneous parcels detected by IF are not detected by OC-SVM) in favor of anomalies related to delay in growth (late

growth, vigorous crop, senescence anomalies). As discussed in Section 4.2.2, it is reasonable to detect heterogeneity issues having a global impact on the crop season before senescence problems, which occurred only at the end of the season. To that extent, results obtained with the LoOP and IF algorithms are more interesting. In what follows, the IF algorithm will be used since its hyperparameters are easy to adjust and it generally provides a better precision (these results were confirmed for a mid season analysis, see Section 4.2.7).

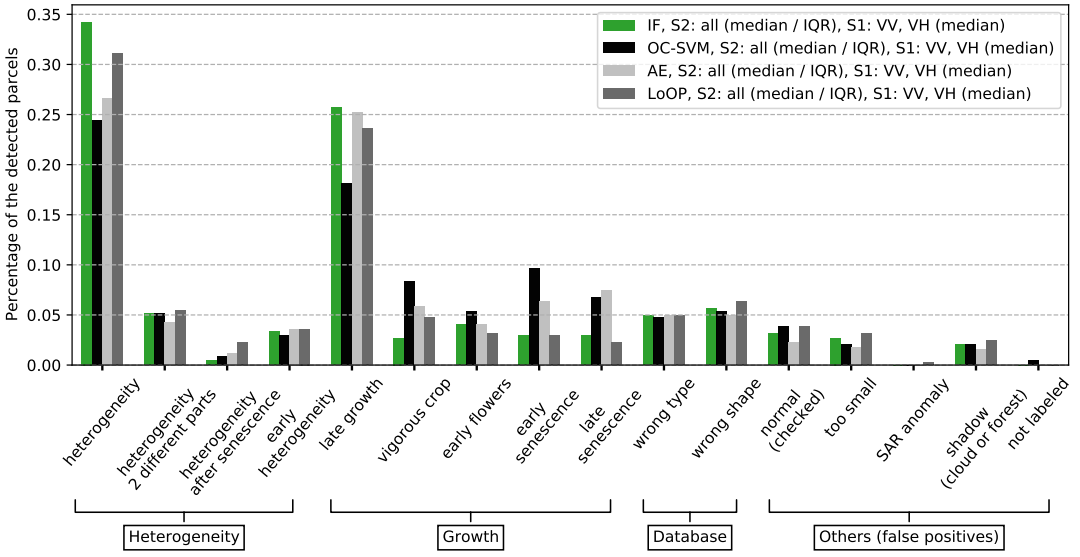

Fig. 12: Percentages of detected parcels within each category for a complete rapeseed growing season analysis. Various outlier detection algorithm are compared with an outlier ratio equal to 20%.

4.2.2. Effect of the feature set used for crop anomaly detection

Fig. 13 shows the precision against outlier ratio for a selection of the best feature sets resulting from S1 and S2 data using the IF algorithm. The best AUC is obtained when using all S1 and S2 indicators jointly. Note that S1 data allow a larger amount of true positives to be detected accurately. However, when using only S2 indicators (or even only NDVI), a similar precision is reached for outlier ratios lower than 30% (even if the percentage of parcels detected in each category is not identical, see details below). Using all S2 indicators instead of NDVI only increases slightly the precision of the results for outlier ratio higher than 40%, confirming that NDVI is relevant to characterize efficiently a growing season but that some anomalies are better described using all 5 VIs. Finally, a lower AUC is obtained when using NDVI and S1 data when compared to the 5 VIs combined with VH and VV.

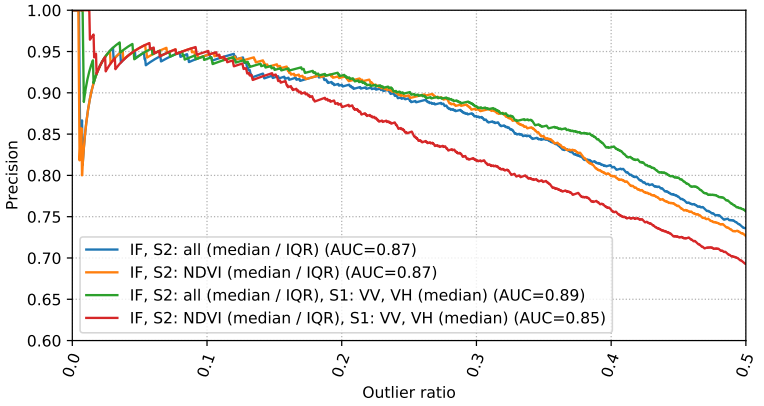

Fig. 13: Precision vs. outlier ratio for a complete growing season analysis of the rapeseed parcels. Various sets of features using the IF algorithm are compared.

In order to complement the results of Fig. 13, the percentages of detected parcels within each category for an outlier ratio of 20% are depicted in Fig. 14. Again, the most frequent anomalies detected are due to heterogeneity and late growth. More growth anomalies (late/vigorous growth) and less heterogeneity are detected when S1 data is used (see also results provided in Section 4.2.5 that confirms this observation). Results obtained when using all S2 indicators or only NDVI are close to each other in this example. However, the subsets of detected parcels by each configuration are not identical (55 parcels detected by one set of features are not detected by the other). Note that more false positives are detected when using NDVI only and S1 indicators, which leads to a precision of 89.4% whereas it is close to 93% for the other features sets. The results of this section confirm the relevance of using median and IQR of all 5 S2 indicators jointly with median of VV and VH S1 indicators for detecting anomalous crop development.

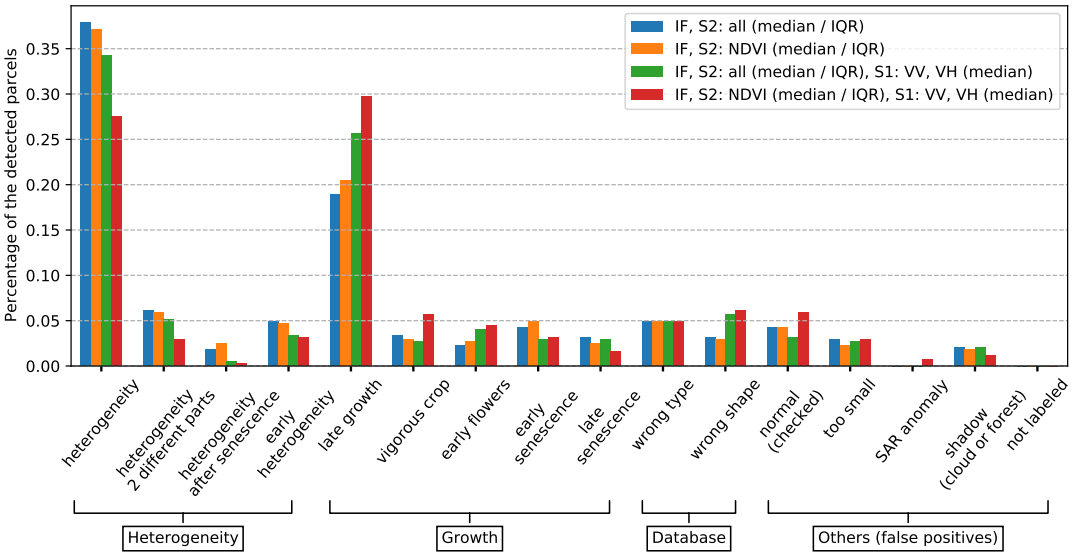

Fig. 14: Percentages of detected parcels within each category for a complete rapeseed growing season analysis. Various sets of features are compared with the IF algorithm and an outlier ratio equal to 20%.

4.2.3. Effect of the outlier ratio

Three experiments were run using the median and IQR statistics derived from S2 images, the median statistics derived from S1 images and the IF algorithm, varying the outlier ratio in $\{0.1, 0.2, 0.3\}$. The percentages of detected parcels in the different anomaly categories for each of these experiments are depicted in Fig. 15. For an outlier ratio of 10%, the detected anomalies are mostly concentrated in wrong types, late growth and global heterogeneity which is relevant and confirms the observations made in Section 4.2.2. Moreover, for this outlier ratio, 45% of the detected parcels belong to the category referred to as "global heterogeneity", which is coherent since this type of anomaly is frequently strongly affecting the crop development of the parcels. Increasing the outlier ratio allows anomalies affecting smaller time periods of the season to be detected, such as early flowering and senescence problems in accordance to the observation made in Section 2.4 during labeling. For an outlier ratio of 30%, much more false positives are detected (parcels labeled as normal). These results show that the IF algorithm provides a relevant anomaly score since more severe anomalies have highest anomaly scores. Moreover, because the score given by IF is computed only once, there is no need to run the algorithm several times when changing the outlier ratio and the amount of parcel to be detected can be easily adapted to the users' needs. Finally, for a generic analysis, choosing an outlier ratio of 20% is a good balance between the precision of the detection results and the amount of parcel to be detected.

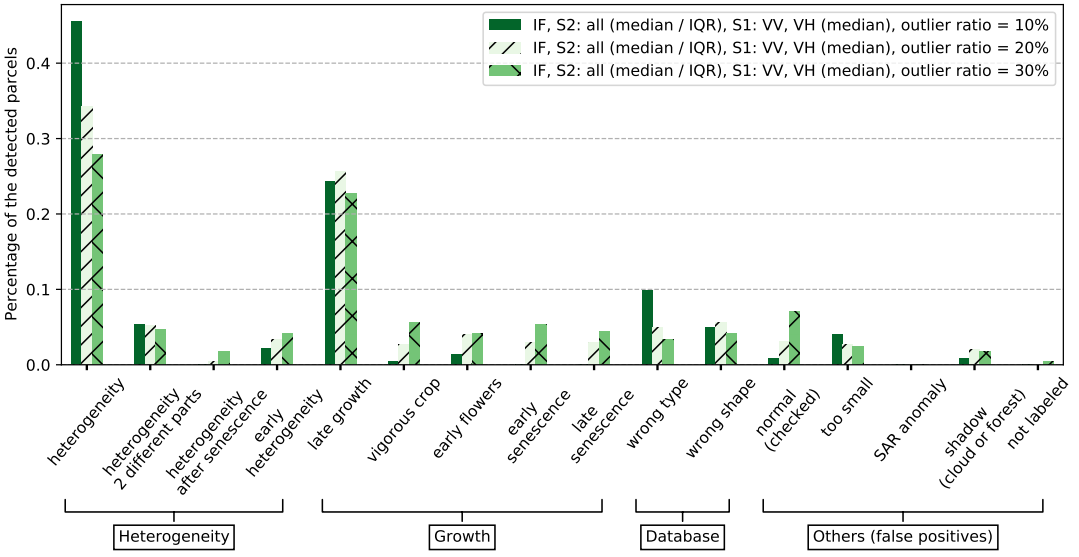

Fig. 15: Percentages of detected parcels within each category for a complete rapeseed growing season analysis. Various outlier ratio are tested with the same set of features and the IF algorithm.

4.2.4. Effect of adding new statistics for S2 data

All the previous experiments were conducted using the median and IQR of S2 data as statistics computed at the parcel-level. This section investigates two new statistics, namely the skewness and kurtosis (*i.e.*, the normalized third and fourth order moments of the indicators). Fig. 16 shows the precision vs. outlier ratio when using the IF algorithm and these two additional statistics computed from S2 images to detect anomalies in rapeseed parcels. All the parcels are labeled for outlier ratios that are at least smaller than 10% (less tests were made with skewness and kurtosis statistics as poor results were obtained). It can be observed in this figure that even for an outlier ratio lower than 5%, using skewness and kurtosis statistics leads to a significant difference in the precision results. One issue encountered when using these new statistics is the detection of too subtle anomalies that are not always related to agronomic anomalies. Using the median only is also tested but provides a lower average precision score. This analysis confirms the importance of IQR statistics, which allows a larger number of relevant anomalies to be detected, and in particular heterogeneity problems. This section showed that using median and IQR statistics of S2 indicators computed at the parcel level is recommended for crop monitoring.

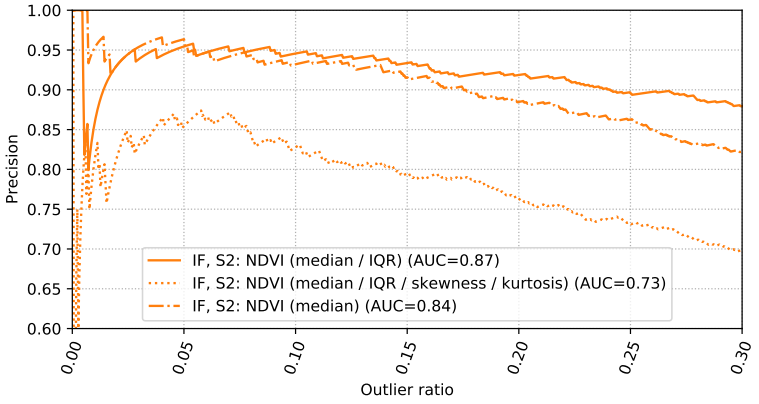

Fig. 16: Precision vs. outlier ratio for a complete growing season analysis of the rapeseed parcels. Various statistics of the NDVI are compared using the IF algorithm.

4.2.5. Using S1 data only

For a complete season analysis, as shown in Section 4.2.2, using S1 data globally increases the precision of the results for a given outlier ratio. Using S1 data alone could be interesting when S2 images are not available (*e.g*, due to presence of clouds). Fig. 17 illustrates various precision vs. outlier ratio curves obtained using S1 images alone and compared to the results obtained when using S1 and S2 indicator jointly. For outlier ratios smaller than 10%, using S1 data alone is sufficient to have a high precision (near 95%). This confirms that outlier scores given by IF to each parcel are relevant since the precision increase when reducing the outlier ratio. Moreover, for a outlier ratios higher than 20%, an acceptable precision near 83% can be reached. Fig. 17 also shows that using the median and IQR statistics for S1 data provides lower AUC, due to the strong correlation between these two statistics. Note finally that the medians of VH and VV polarization were also tested separately (not displayed here) without any improvement, confirming that both polarization are relevant for outlier detection.

The distribution of the detected anomalies in each category is depicted in Fig. 18. For this experiment, the outlier ratio was fixed to 10% because higher values yield results with a lower precision, as shown in Fig. 17. It can be observed that S1 data are less adapted to detect heterogeneity problems, which explain why it was difficult to detect a large amount of relevant anomalies using S1 data only (the SAR sensor is sensitive to the structure of the vegetation). However, the use of S1 data is interesting to detect vigorous crops (that are almost not detected here with S2) and growth anomalies in general. It can be observed that when adding the IQR statistics computed on S1 data, more late growth parcels (20 parcels) and fewer vigorous crop parcels are detected. These results confirm that median statistics

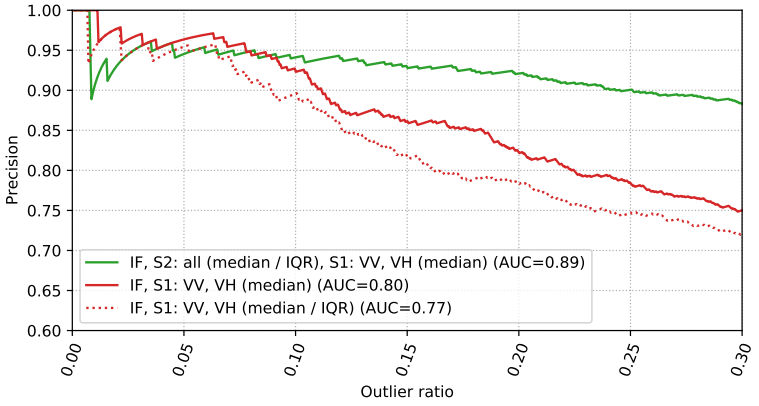

Fig. 17: Precision vs. outlier ratio for a complete growing season analysis of the rapeseed parcels. Various sets of features are compared.

of VV and VH S1 indicators are relevant for crop monitoring and stress out the potential interest of using S1 data only when no S2 images is available.

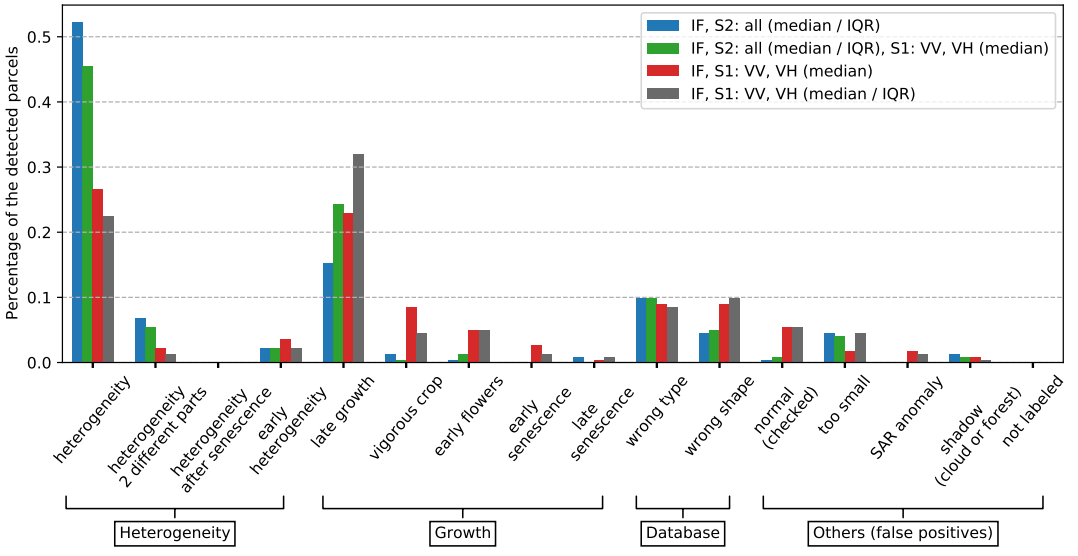

Fig. 18: Percentages of detected parcels within each category for a complete growing season analysis of rapeseed parcels with the IF algorithm. Outlier ratio is equal to 10%.

4.2.6. *Effect of missing S2 images*

Two scenarios were investigated to evaluate the effect of missing S2 images.

- Scenario 1: the proposed approach was investigated using 6 S2 images instead of 13 to analyze the influence of a reduced amount of S2 images thorough the season. Only 1 image out of 2 was considered for the detection (the first S2 image was not used, the second S2 image was used and so on). Precision vs. outlier ratio curves are presented in Fig. 19, where it can be observed that the proposed method is robust to missing S2 images.

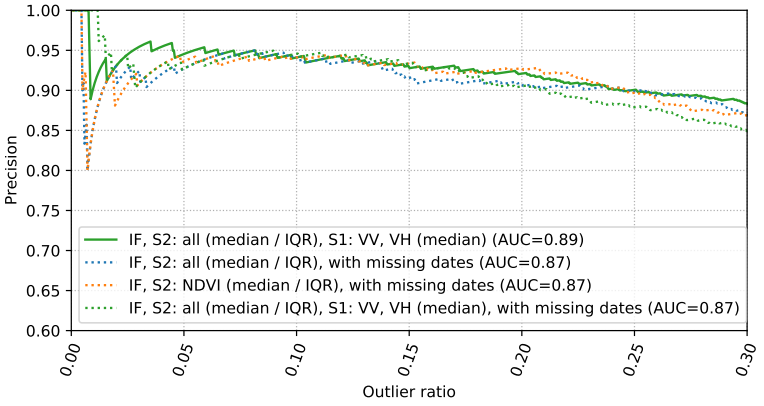

Fig. 19: Precision vs. outlier ratio for a complete season analysis of the rapeseed dataset. Missing dates means that only 1 S2 images out of 2 was taken (6 S2 images instead of 13).

- Scenario 2: another experiment was conducted to evaluate the effect of missing S2 images during the first part of the growing season (e.g, more clouds during winter). Precisely, we consider only 7 dates of S2 data between May and June that are used jointly with all S1 images. Precision vs. outlier ratio curves are presented in Fig. 20. In that case, using S1 images improve significantly the precision of the results. The reason is that using S1 allows the algorithm to detect almost the same amount of late growth crops when compared to using a complete season of S2 images which is logical since S1 data are well suited to detect growth anomalies. These results confirm the interest of using S1 data as a complement to S2 sparse time series.

4.2.7. *Mid-season analysis*

A mid-season analysis (using only dates before February) was conducted for multiple reasons detailed in Section 3.6. A first experiment was made with the best sets of features selected in Section 4.2.2 for a complete season analysis using rapeseed parcels. Results displayed in Fig. 21 show that even with

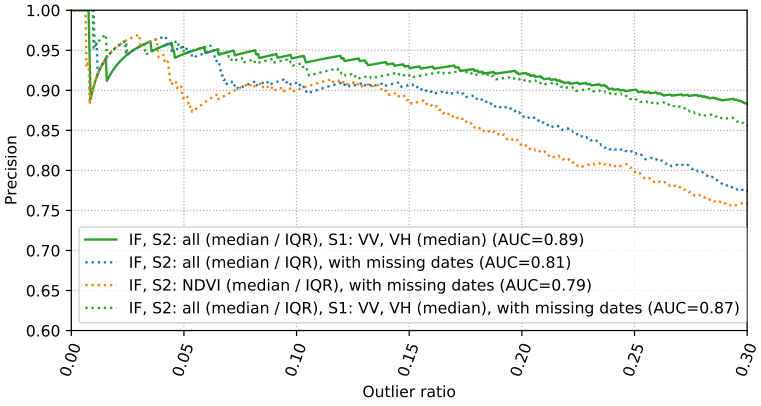

Fig. 20: Precision vs. outlier ratio for complete season analysis of the rapeseed dataset. Missing dates means that only the S2 images acquired after April were used (7 images).

a small number of images, many agronomic anomalies are detected (best precision=87.7% for an outlier ratio equal to 20%). This confirms the previous results found in the case of missing S2 images. Fig. 21 also shows that the best results are again obtained using all S1 and S2 indicators jointly with a higher average precision since more actual anomalies detected for larger outlier ratios (*e.g.*, the precision is 5% better for an outlier ratio fixed to 30%).

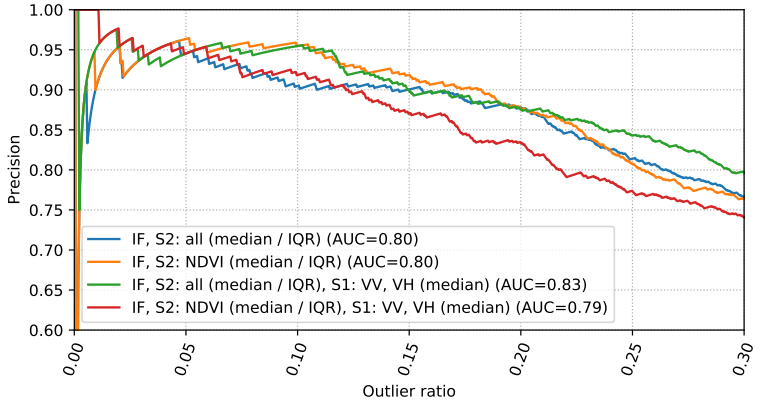

Fig. 21: Precision vs. outlier ratio for a mid-season analysis of rapeseed parcels (all images available before February). Various sets of features are compared using the IF algorithm.

The impact of a mid-season analysis regarding the different categories of detected anomalies is depicted in Fig. 22. In this case, almost no senescence problems are detected, which is easy to understand. Even with only 3 S2 images acquired between October and December, most other agronomic anomalies are detected by the algorithm. A mid-season analysis is able to detect more late growth anomalies and fewer heterogeneous parcels because late growth is impacting mostly the beginning of

the season (especially for rapeseed crops). Finally, more false positives are detected with a mid-season analysis, which can be understood since the amount of potential anomalies to be detected is lower.

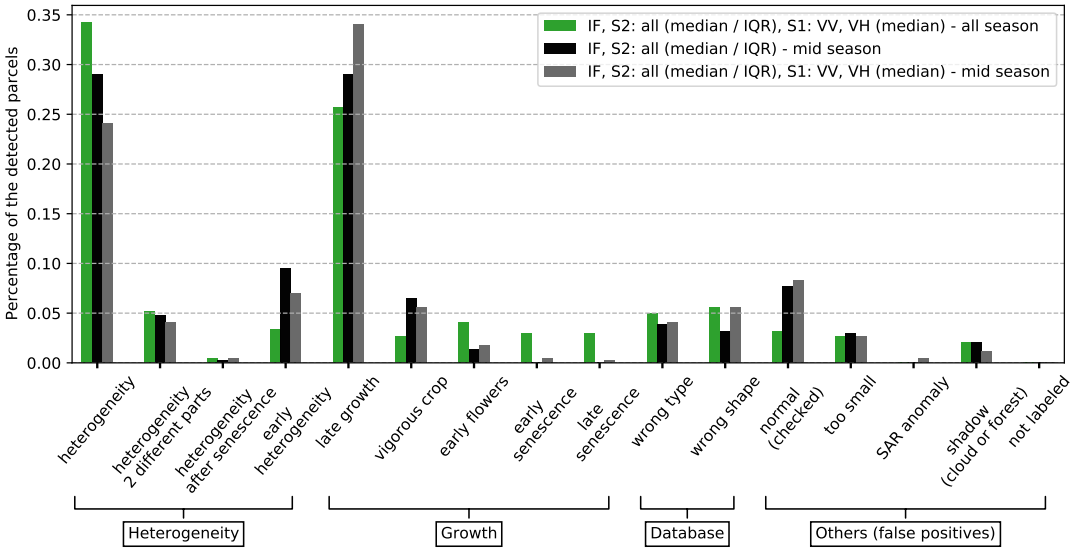

Fig. 22: Percentages of detected parcels within each category in the rapeseed dataset. Results obtained for a mid season analysis (before February) and a complete growing season analysis are compared for a outlier ratio equal to 10%.

Complementary results for a mid season analysis are briefly presented in what follows since they confirm the observations made for a complete growing season analysis. The IF algorithm provides overall better results (AUC=0.83) and is more robust to changes. The AE performs slightly worse than IF (AUC=0.81), especially for outlier ratios greater than 20%. OCSV (AUC=0.79) and LoOP (AUC=0.77) perform significantly worse in this case. These differences in performance can be explained by the fact that the parameters of OC-SVM, LoOP and AE algorithms are more difficult to tune compared to the IF algorithm. Regarding the influence of the outlier ratio, as for a complete season analysis increasing its value logically leads to detect more subtle anomalies (i.e., affecting a limited time interval) and more false positives, which confirms the relevance of the anomaly score given by IF. Almost no early heterogeneity and vigorous crop is detected with an outlier ratio of 10%. Early heterogeneity is a more subtle anomaly than global heterogeneity, which confirms separation between these two categories. Finally, when using S1 data only, the detection results obtained for an outlier ratio of 10% are still accurate with a precision equal to 89.6%. These results confirm that S1 images are adapted to an early season analysis, especially thanks to an easier detection of late growth problems.

4.3. Extension to wheat crops (2016/2017)

A complementary analysis was made to measure the robustness of the proposed method to a change in the crop type. An experiment is presented with the selection of the best features used for rapeseed crops analysis. The IF algorithm was used to detect abnormal wheat parcels for a complete growing season with an outlier ratio of 10%. The percentage of detected anomalies withing each category is shown in Fig. 23, which also indicates the precision obtained for each detection since the precision vs. outlier ratio curves are not displayed here. Again, combining S1 and S2 data leads to the best precision (95.5%). Similar to rapeseed crops, using S1 data allows more growth anomalies to be detected when compared to S2 data alone. Using all 5 S2 indicators instead of NDVI allows the number of detected vigorous crops to be increased (12 parcels) since NDVI can saturate for high values. The precision obtained using S1 data alone is lower due to a higher number of SAR anomalies (i.e., 22 SAR anomalies) but the results are still accurate (precision=86.9%). As for the rapeseed analysis, no SAR anomaly is detected when using S1 and S2 data jointly. These results confirm the interest of the proposed approach and its robustness to changes in the crop type. Finally, note that some experiments were conducted for a mid-season analysis and are in agreement with those obtained with rapeseed parcels.

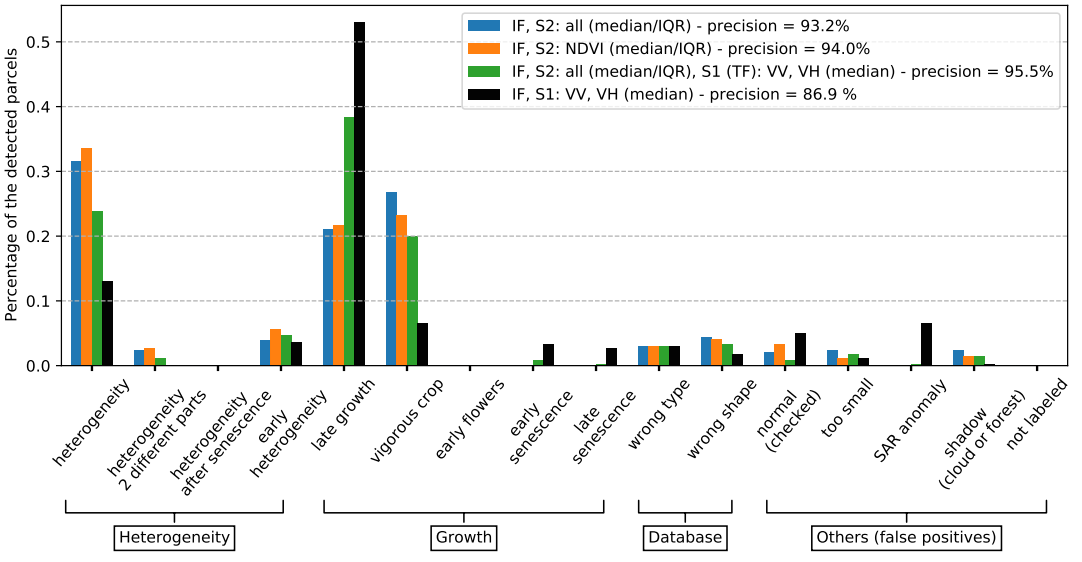

Fig. 23: Percentage of detected anomalies within each category for the wheat parcel (complete growing season). Various sets of features are compared with an outlier ratio equal to 10%.

5. Conclusion

This paper studied a new anomaly detection method for crop monitoring. This method is decomposed in 4 main steps: 1) preprocessing of multispectral and synthetic aperture radar (SAR) images (Sentinel-1 and Sentinel-2 images were used in this study), 2) computation of vegetation indicators (5 multispectral indicators and 2 SAR indicators that are listed below), 3) computation of zonal statistics at the parcel-level for each indicator at each date (more precisely, medians and IQRs for the multispectral indicators and medians for the SAR indicators for each parcel), 4) detection of abnormal crop parcel using an outlier detection algorithm fed by the multi-temporal zonal statistics (we recommend here to use the isolation forest algorithm for its simplicity and robustness). The proposed method is fully unsupervised and can be used without a large amount of historical data. It can be applied to different kinds of crops (such as rapeseed or wheat considered in this paper) and is able to detect a majority of parcels that are abnormal in an agronomic sense. Moreover, a relevant anomaly score can be defined for each parcel allowing the importance of this anomaly to be quantified.

This study shows that multi-temporal vegetation indices computed at the parcel-level from multispectral images (such as Sentinel-2 images) provide relevant results for detecting anomalies in crops. These indices include the Normalized Difference Vegetation Index (NDVI), which can detect a majority of agronomic anomalies. Adding other indicators such as the Green-Red Vegetation Index (GRVI), two variants of the Normalized Difference Water Index (NDWI) and a variant of the Modified Chlorophyll Absorption Ratio Index (MCARI/OSAVI) allows additional and more subtle anomalies to be detected. Using VV and VH backscattering coefficients indicators extracted from SAR images (such as Sentinel-1 images) jointly with multispectral indicators generally provided the best results, detecting some anomalies difficult to detect with S2 data only. Moreover, when an important part of the season misses multispectral images (such as the growing phase at the beginning of the season), SAR data are complementary to multispectral images and help to detect growth anomalies. Using SAR images only can be suited for cloudy regions with few available multispectral images. However, it was observed that heterogeneity problems are more difficult to detect with SAR images only, even if strongly heterogeneous parcels are still detected.

Spatial statistics computed at a parcel-level reduce the computational complexity of the algorithm and summarize efficiently the information regarding the analyzed parcels. More precisely, median and interquartile range (IQR) of vegetation indices (capturing the mean and dispersion of the indicators)

computed at a parcel-level can be used efficiently for crop anomaly detection. An interesting property of the proposed method is its robustness to parcellation errors, which confirms that a parcel-level approach with robust statistics is adapted to crop monitoring.

Outlier detection techniques applied to zonal statistics are well suited to detect agronomic anomalies in crops, in an unsupervised way without a need for a large amount of historical data. Among all the tested outlier detection methods, the isolation forest algorithm provided more consistent results with a simple hyperparameter tuning.

Further investigation should be conducted to determine whether other indicators, *e.g.*, using biophysical indicators such as the Leaf Area Index (LAI) or the fraction of green vegetation cover (fCover) (Djamai et al., 2019; Verrelst et al., 2015b), can improve anomaly detection results. Regarding SAR indicators, the use of SLC images could also be investigated to extract polarimetric parameters such as entropy or volume scattering. Another line of research is to take into account the temporal structure of vegetation indices to potentially improve detection of agronomic anomalies and estimate the dates where the detected anomalies have appeared. For instance, contextual outlier detection might be interesting for disturbance or inter-annual anomaly detection. Including a contextual outlier detection in the proposed strategy might provide complementary information to detect both inter-annual and intra-annual anomalies. Coupling the proposed detection method with a supervised or unsupervised classification algorithm is another prospect, in order to assign to each detection an anomaly type that could be helpful for users, for example to identify heterogeneity or growth problems. It could also be interesting to investigate other types of crops such as soybean (a low biomass crop contrary to wheat and rapeseed that are both considered as high biomass crops). Finally, an anomaly map could possibly be generated for large areas, by taking for instance large rectangular windows of vegetation status.

6. Acknowledgements

The authors would like to thanks Alexandre Bouvet, Milena Planells and their colleagues from CESBIO (Centre d'Etudes Spatiales de la BIOsphère) for the help regarding the processing of S1 images.

Appendix A Supplementary material

Supplementary data to this article can be found in the document provided in complement of the manuscript.

References

Abdikan, S., Balik Sanli, F., Üstüner, M., Calò, F., 2016. Land cover mapping using Sentinel-1 SAR data, in: Proc. ISPRS, Prague, Czech Republic. pp. 757–761. doi:10.5194/isprs-archives-XLI-B7-757-2016.

Aggarwal, C.C., 2017a. Linear Models for Outlier Detection. Springer International Publishing, Cham. chapter 3. p. 93. doi:10.1007/978-3-319-47578-3_3.

Aggarwal, C.C., 2017b. Outlier Analysis. 2nd ed., Springer International Publishing, Cham. doi:10.1007/978-3-319-47578-3_3.

Albughdadi, M., Kouamé, D., Rieu, G., Tourneret, J.Y., 2017. Missing data reconstruction and anomaly detection in crop development using agronomic indicators derived from multispectral satellite images, in: Proc. IEEE IGARSS, Fort Worth, TX, USA. pp. 5081–5084. doi:10.1109/IGARSS.2017.8128145.

An, J., Cho, S., 2015. Variational autoencoder based anomaly detection using reconstruction probability. Technical Report. SNU Data Mining Center.

Atzberger, C., Eilers, P.H.C., 2011. Evaluating the effectiveness of smoothing algorithms in the absence of ground reference measurements. Int. J. Remote Sens. 32, 3689–3709.

Bannari, A., Morin, D., Bonn, F., Huete, A.R., 1995. A review of vegetation indices. Remote Sensing Reviews 13, 95–120. doi:10.1080/02757259509532298.

Beck, P.S., Atzberger, C., Høgda, K.A., Johansen, B., Skidmore, A.K., 2006. Improved monitoring of vegetation dynamics at very high latitudes: A new method using MODIS NDVI. Remote Sens. Environ. 100, 321–334.

Betbeder, J., Rémy, F., Philippets, Y., Ferro-Famil, L., Baup, F., 2016. Contribution of multitemporal polarimetric synthetic aperture radar data for monitoring winter wheat and rapeseed crops. J. Appl. Remote Sens. 10, 026020. doi:10.1117/1.JRS.10.026020.

Borg, I., Groenen, P., 1997. Modern Multidimensional Scaling. Springer-Verlag New York.

Breunig, M., Kriegel, H.P., Ng, R.T., Sander, J., 2000. LOF: Identifying density-based local outliers, in: Proc. ACM SIGMOD, Dallas, TX, USA. pp. 93–104.

Chandola, V., Banerjee, A., Kumar, V., 2009. Survey of anomaly detection. ACM Comput. Surveys 41, 15:1–15:58.

Constantinou, V., 2018. PyNomaly: Anomaly detection using local outlier probabilities (LoOP). J. Open Source Softw. 3, 845. doi:10.21105/joss.00845.

Daughtry, C., Walthall, C., Kim, M., de Colstoun, E., McMurtrey, J., 2000. Estimating corn leaf chlorophyll concentration from leaf and canopy reflectance. Remote Sens. Environ. 74, 229 – 239. doi:https://doi.org/10.1016/S0034-4257(00)00113-9.

Defourny, P., Bontemps, S., Bellemans, N., Cara, C., Dedieu, G., Guzzonato, E., Hagolle, O., Inglada, J., Nicola, L.,

Rabaute, T., Savinaud, M., Udroiu, C., Valero, S., Bégué, A., Dejoux, J.F., Harti], A.E., Ezzahar, J., Kussul, N., Labbassi, K., Lebourgeois, V., Miao, Z., Newby, T., Nyamugama, A., Salh, N., Shelestov, A., Simonneaux, V., Traore, P.S., Traore, S.S., Koetz, B., 2019. Near real-time agriculture monitoring at national scale at parcel resolution: Performance assessment of the Sen2-Agri automated system in various cropping systems around the world. Remote Sens. Environ. 221, 551 – 568. URL: http://www.sciencedirect.com/science/article/pii/S0034425718305145, doi:https://doi.org/10.1016/j.rse.2018.11.007.

Denize, J., Hubert-Moy, L., Betbeder, J., Corgne, S., Baudry, J., Pottier, E., 2018. Evaluation of using Sentinel-1 and Sentinel-2 time-series to identify winter land use in agricultural landscapes. Remote Sens. 11. URL: https://www.mdpi.com/2072-4292/11/1/37.

Djamai, N., Fernandes, R., Weiss, M., McNairn, H., Goïta, K., 2019. Validation of the Sentinel simplified Level 2 product prototype processor (SL2P) for mapping cropland biophysical variables using Sentinel-2/MSI and Landsat-8/OLI data. Remote Sensing of Environment 225, 416 – 430. URL: http://www.sciencedirect.com/science/article/pii/S0034425719301117, doi:https://doi.org/10.1016/j.rse.2019.03.020.

Drusch, M., Del Bello, U., Carlier, S., Colin, O., Fernandez, V., Gascon, F., Hoersch, B., Isola, C., Laberinti, P., Martimort, P., Meygret, A., Spoto, F., Sy, O., Marchese, F., Bargellini, P., 2012. Sentinel-2: ESA's optical high-resolution mission for GMES operational services. Remote Sensing of Environment 120, 25 – 36. URL: http://www.sciencedirect.com/science/article/pii/S0034425712000636, doi:https://doi.org/10.1016/j.rse.2011.11.026. the Sentinel Missions - New Opportunities for Science.

Filipponi, F., 2019. Sentinel-1 GRD preprocessing workflow, in: Proc. ECRS-3, MDPI AG. p. 11. doi:10.3390/ecrs-3-06201.

Gao, B., 1996. NDWI — A normalized difference water index for remote sensing of vegetation liquid water from space. Remote Sens. Environ. 58, 257 – 266. doi:https://doi.org/10.1016/S0034-4257(96)00067-3.

Gómez, C., White, J.C., Wulder, M.A., 2016. Optical remotely sensed time series data for land cover classification: A review. ISPRS J. Photogramm. Remote Sens. 116, 55 – 72. URL: http://www.sciencedirect.com/science/article/pii/S0924271616000769, doi:https://doi.org/10.1016/j.isprsjprs.2016.03.008.

Hagolle, O., Huc, M., Villa Pascual, D., Dedieu, G., 2015. A multi-temporal and multi-spectral method to estimate aerosol optical thickness over land, for the atmospheric correction of Formosat-2, Landsat, VENμS and Sentinel-2 images. Remote Sens. 7, 2668–2691. URL: https://www.mdpi.com/2072-4292/7/3/2668, doi:10.3390/rs70302668.

Hedayati, P., Bargiel, D., 2018. Fusion of Sentinel-1 and Sentinel-2 images for classification of agricultural areas using a novel classification approach, in: Proc. IEEE IGARSS, Valencia, Spain. pp. 6643–6646. doi:10.1109/IGARSS.2018.8518327.

Huber, P.J., 2011. Robust Statistics. Springer Berlin Heidelberg, Berlin, Heidelberg. pp. 1248–1251. URL: https://doi.org/10.1007/978-3-642-04898-2_594, doi:10.1007/978-3-642-04898-2_594.

Inglada, J., Vincent, A., Arias, M., Marais-Sicre, C., 2016. Improved early crop type identification by joint use of high temporal resolution SAR and optical image time series. Remote Sens. 8, 362. URL: http://dx.doi.org/10.3390/rs8050362, doi:10.3390/rs8050362.

Inglada, J., Vincent, A., Arias, M., Tardy, B., Morin, D., Rodes, I., 2017. Operational high resolution land cover map produc-

tion at the country scale using satellite image time series. Remote Sens. 9, 95. URL: http://dx.doi.org/10.3390/rs9010095, doi:10.3390/rs9010095.

J. Verbesselt, A. Zeileis, M.H., 2012. Near real-time disturbance detection using satellite image time series. Remote Sens. Environ. 123, 98 – 108.

Jaakkola, T., Diekhans, M., Haussler, D., 1999. Using the Fisher kernel method to detect remote protein homologies, in: ISMB, AAAI Press, Menio Park, CA, USA. pp. 149–158.

Jolliffe, I.T., 1986. Principal Component Analysis. Springer New York, New York, NY. doi:10.1007/978-1-4757-1904-8_8.

Kanjir, U., Đurić, N., Veljanovski, T., 2018. Sentinel-2 based temporal detection of agricultural land use anomalies in support of common agricultural policy monitoring. ISPRS International Journal of Geo-Information 7, 405. doi:10.3390/ijgi7100405.

Khabbazan, S., Vermunt, P., Steele-Dunne, S., Ratering Arntz, L., Marinetti, C., van der Valk, D., Iannini, L., Molijn, R., Westerdijk, K., van der Sande, C., 2019. Crop monitoring using Sentinel-1 data: A case study from the Netherlands. Remote Sens. 11. URL: https://www.mdpi.com/2072-4292/11/16/1887, doi:10.3390/rs11161887.

Klisch, A., Atzberger, C., 2016. Operational drought monitoring in Kenya using MODIS NDVI time series. Remote Sens. 8, 267.

Kramer, M.A., 1991. Nonlinear principal component analysis using autoassociative neural networks. AIChE Journal 37, 233–243. doi:10.1002/aic.690370209.

Kriegel, H.P., Kröger, P., Schubert, E., Zimek, A., 2009. LoOP: Local outlier probabilities, in: Proc. CIKM, Honk Kong, China. pp. 1649–1652. doi:10.1145/1645953.1646195.

Kumar, D., Rao, S., Sharma, J., 2013. Radar vegetation index as an alternative to NDVI for monitoring of soyabean and cotton, in: Proc. INCA, Jodhpur, India. pp. 91–96.

Kuo, B., Ho, H., Li, C., Hung, C., Taur, J., 2014. A kernel-based feature selection method for SVM with RBF kernel for hyperspectral image classification. IEEE Journal of Selected Topics in Applied Earth Observations and Remote Sensing 7, 317–326. doi:10.1109/JSTARS.2013.2262926.

Kussul, N., Mykola, L., Shelestov, A., Skakun, S., 2018. Crop inventory at regional scale in Ukraine: developing in season and end of season crop maps with multi-temporal optical and SAR satellite imagery. European Journal of Remote Sensing 51, 627–636. doi:10.1080/22797254.2018.1454265.

LeCun, Y., Bengio, Y., Hinton, G., 2015. Deep learning. Nature 521, 436–44. doi:10.1038/nature14539.

Liu, C., Chen, Z., Shao, Y., Chen, J., Hasi, T., Pan, H., 2019. Research advances of SAR remote sensing for agriculture applications: A review. J. Integr. Agric. 18, 506 – 525. URL: http://www.sciencedirect.com/science/article/pii/S2095311918620167, doi:https://doi.org/10.1016/S2095-3119(18)62016-7.

Liu, F.T., Ting, K.M., Zhou, Z., 2008. Isolation forest, in: IEEE ICDM, Pisa, Italy. pp. 413–422. doi:10.1109/ICDM.2008.17.

Liu, F.T., Ting, K.M., Zhou, Z.H., 2012. Isolation-based anomaly detection. ACM Trans. Knowl. Discov. Data 6. doi:10.1145/2133360.2133363.

Marzahn, P., Wegmuller, U., Mattia, F., Ludwig, R., 2012. “flashing fields” and the impact of soil surface roughness, in: Proc.

IEEE IGARSS, Munich, Germany. pp. 6963–6966. doi:10.1109/IGARSS.2012.6351968.

McFeeters, S.K., 1996. The use of the normalized difference water index (NDWI) in the delineation of open water features. Int. J. Remote Sens. 17, 1425–1432. doi:10.1080/01431169608948714.

McNairn, H., Shang, J., 2016. A review of multitemporal synthetic aperture radar (SAR) for crop monitoring, in: Ban, Y. (Ed.), Multitemporal Remote Sensing: Methods and Applications. Springer International Publishing, Cham, Switzerland. chapter 15, pp. 317–340. doi:10.1007/978-3-319-47037-5_15.

Meroni, M., Fasbender, D., Rembold, F., Atzberger, C., Klisch, A., 2019. Near real-time vegetation anomaly detection with MODIS NDVI: Timeliness vs. accuracy and effect of anomaly computation options. Remote Sens. Environ. 221, 508–521.

Moran, M.S., Hymer, D.C., Qi, J., Sano, E.E., 2000. Soil moisture evaluation using multi-temporal synthetic aperture radar (SAR) in semiarid rangeland. Agric. For. Meteorol. 105, 69 – 80. URL: http://www.sciencedirect.com/science/article/pii/S0168192300001891, doi:https://doi.org/10.1016/S0168-1923(00)00189-1.

Motohka, T., Nasahara, K.N., Oguma, H., Tsuchida, S., 2010. Applicability of green-red vegetation index for remote sensing of vegetation phenology. Remote Sens. 2, 2369–2387. URL: https://www.mdpi.com/2072-4292/2/10/2369, doi:10.3390/rs2102369.

Navarro, A., Rolim, J., Miguel, I., Catalão, J., Silva, J., Painho, M., Vekerdy, Z., 2016. Crop monitoring based on SPOT-5 Take-5 and Sentinel-1A data for the estimation of crop water requirements. Remote Sens. 8, 525. doi:10.3390/rs8060525.

Pedregosa, F., Varoquaux, G., Gramfort, A., Michel, V., Thirion, B., Grisel, O., Blondel, M., Prettenhofer, P., Weiss, R., Dubourg, V., Vanderplas, J., Passos, A., Cournapeau, D., Brucher, M., Perrot, M., Duchesnay, E., 2011. Scikit-learn: Machine learning in Python. J. Mach. Learn. Res. 12, 2825–2830.

Pimentel, M., Clifton, D., Clifton, L., Tarassenko, L., 2014. A review of novelty detection. Signal Process. 99, 215–249.

Prendes, J., Chabert, M., Pascal, F., Giros, A., Tourneret, J.Y., 2015a. Change detection for optical and radar images using a Bayesian nonparametric model coupled with a Markov random field, in: Proc. IEEE Int. Conf. Acoust., Speech, and Signal Proc., Brisbane, Australia. pp. 1513–1517.

Prendes, J., Chabert, M., Pascal, F., Giros, A., Tourneret, J.Y., 2015b. A new multivariate statistical model for change detection in images acquired by homogeneous and heterogeneous sensors. IEEE Trans. Image Process. 24, 799–812.

Prendes, J., Chabert, M., Pascal, F., Giros, A., Tourneret, J.Y., 2015c. Performance assessment of a recent change detection method for homogeneous and heterogeneous images. Revue Française de Photogrammétrie et de Télédétection 209, 23–29.

Quegan, S., Jiong Jiong Yu, 2001. Filtering of multichannel SAR images. IEEE Trans. Geosci. Remote Sens. 39, 2373–2379. doi:10.1109/36.964973.

Rouse, J., Haas, R., Schell, J., Deering, D., 1974. Monitoring vegetation systems in the great plains with ERTS. NASA special publication 351, 309.

Schölkopf, B., Tsuda, K., Vert, J.P., 2004. Kernel methods in computational biology. MIT Press, Cambridge, Mass.

Schölkopf, B., Williamson, R., Smola, A., Shawe-Taylor, J., Platt, J., 1999. Support vector method for novelty detection, in: Proc. NIPS, Denver, CO, USA. pp. 582–588.

Tax, D.M.J., Duin, R.P.W., 2004. Support vector data description. Mach. Learn. 54, 45–66. URL: https://doi.org/10.1023/B:MACH.0000008084.60811.49, doi:10.1023/B:MACH.0000008084.60811.49.

Veloso, A., Mermoz, S., Bouvet, A., Toan, T.L., Planells, M., Dejoux, J.F., Ceschia, E., 2017. Understanding the temporal behavior of crops using Sentinel-1 and Sentinel-2-like data for agricultural applications. Remote Sensing of Environment 199, 415 – 426. URL: http://www.sciencedirect.com/science/article/pii/S0034425717303309, doi:https://doi.org/10.1016/j.rse.2017.07.015.

Verrelst, J., Camps-Valls, G., Muñoz-Marí, J., Rivera, J.P., Veroustraete, F., Clevers, J.G., Moreno, J., 2015a. Optical remote sensing and the retrieval of terrestrial vegetation bio-geophysical properties – a review. ISPRS J. Photogramm. Remote Sens. 108, 273 – 290. URL: http://www.sciencedirect.com/science/article/pii/S0924271615001422, doi:https://doi.org/10.1016/j.isprsjprs.2015.05.005.

Verrelst, J., Rivera, J.P., Veroustraete, F., Muñoz-Marí, J., Clevers, J.G., Camps-Valls, G., Moreno, J., 2015b. Experimental Sentinel-2 LAI estimation using parametric, non-parametric and physical retrieval methods – a comparison. ISPRS J. Photogramm. Remote Sens. 108, 260 – 272. URL: http://www.sciencedirect.com/science/article/pii/S0924271615001239, doi:https://doi.org/10.1016/j.isprsjprs.2015.04.013.

Virtanen, P., Gommers, R., Oliphant, T.E., Haberland, M., Reddy, T., Cournapeau, D., Burovski, E., Peterson, P., Weckesser, W., Bright, J., van der Walt, S.J., Brett, M., Wilson, J., Jarrod Millman, K., Mayorov, N., Nelson, A.R.J., Jones, E., Kern, R., Larson, E., Carey, C., Polat, İ., Feng, Y., Moore, E.W., Vand erPlas, J., Laxalde, D., Perktold, J., Cimrman, R., Henriksen, I., Quintero, E.A., Harris, C.R., Archibald, A.M., Ribeiro, A.H., Pedregosa, F., van Mulbregt, P., Contributors, S..., 2020. SciPy 1.0: Fundamental Algorithms for Scientific Computing in Python. Nature Methods doi:https://doi.org/10.1038/s41592-019-0686-2.

Vreugdenhil, M., Wagner, W., Bauer-Marschallinger, B., Pfeil, I., Teubner, I., Rüdiger, C., Strauss, P., 2018. Sensitivity of Sentinel-1 backscatter to vegetation dynamics: An Austrian case study. Remote Sens. 10, 1396. doi:10.3390/rs10091396.

Wegmuller, U., Cordey, R.A., Werner, C., Meadows, P.J., 2006. "Flashing Fields" in nearly simultaneous ENVISAT and ERS-2 C-band SAR images. IEEE Trans. Geosci. Remote Sens. 44, 801–805.

Wegmuller, U., Werner, C., 1997. Retrieval of vegetation parameters with SAR interferometry. IEEE Trans. Geosci. Remote Sens. 35, 18–24. doi:10.1109/36.551930.

Wegmüller, U., Santoro, M., Mattia, F., Balenzano, A., Satalino, G., Marzahn, P., Fischer, G., Ludwig, R., Floury, N., 2011. Progress in the understanding of narrow directional microwave scattering of agricultural fields. Remote Sens. Environ. 115, 2423–2433.

Weiss, M., Jacob, F., Duveiller, G., 2020. Remote sensing for agricultural applications: A meta-review. Remote Sens. Environ. 236, 111402. URL: http://www.sciencedirect.com/science/article/pii/S0034425719304213, doi:https://doi.org/10.1016/j.rse.2019.111402.

Whelen, T., Siqueira, P., 2018. Time-series classification of Sentinel-1 agricultural data over North Dakota. Remote Sens. Lett. 9, 411–420. doi:10.1080/2150704X.2018.1430393.

Wu, C., Niu, Z., Tang, Q., Huang, W., 2008. Estimating chlorophyll content from hyperspectral vegetation indices: Modeling and validation. Agric. For. Meteorol. 148, 1230 – 1241. doi:https://doi.org/10.1016/j.agrformet.2008.03.005.

Zhao, Y., Nasrullah, Z., Li, Z., 2019. PyOD: A Python toolbox for scalable outlier detection. Journal of Machine Learning Research 20, 1–7. URL: http://jmlr.org/papers/v20/19-011.html.